

An Asymptotic-Preserving Monte Carlo Method for the Boltzmann Equation[☆]

Wei Ren^a, Hong Liu^{a,*}, Shi Jin^{b,c}

^a*J C Wu Center for Aerodynamics, School of Aeronautics and Aerospace, Shanghai Jiao Tong University, 800 Dong Chuan Road, Shanghai 200240, China*

^b*Department of Mathematics, Institute of Natural Sciences and MOE Key Lab in Scientific and Engineering Computing, Shanghai Jiao Tong University, 800 Dong Chuan Road, Shanghai 200240, China*

^c*Department of Mathematics, University of Wisconsin-Madison, 480 Lincoln Drive, Madison, WI 53706, USA*

Abstract

In this work, we propose an asymptotic-preserving Monte Carlo method for the Boltzmann equation that is more efficient than the currently available Monte Carlo methods in the fluid dynamic regime. This method is based on the successive penalty method [39], which is an improved BGK-penalization method originally proposed by Filbet-Jin [16]. Here we introduce the Monte-Carlo implementation of the method, which, despite of its lower order accuracy, is very efficient in higher dimensions or simulating some complicated chemical processes. This method allows the time step independent of the mean free time which is prohibitively small in the fluid dynamic regime. We study some basic properties of this method, and compare it with some other asymptotic-preserving Monte Carlo methods in terms of numerical performance in different regimes, from rarefied to fluid dynamic regimes, and their computational efficiency.

Keywords: Boltzmann equation, asymptotic preserving scheme, successive-penalty, DSMC

1. Introduction

1.1. Background: numerical methods for the Boltzmann equation

In the study of flows which span a wide range of flow regimes, i.e. in atmospheric re-entry problems, the density distribution $f(t, x, v)$ of a dilute gas at position x , with velocity v and at time t , is governed by the Boltzmann equation [5, 9]:

$$\frac{\partial f}{\partial t} + v \cdot \nabla_x f = \frac{1}{\varepsilon} Q(f, f), \quad x \in \mathbb{R}^{d_x}, \quad v \in \mathbb{R}^{d_v}. \quad (1.1)$$

In Eqn. (1.1), the bilinear collision operator $Q(f, f)$ describes the binary collisions of the particles and is defined by

$$Q(f, f)(v) = \int_{\mathbb{R}^{d_v}} \int_{\mathbb{S}^{d_v-1}} \sigma(|v - v_1|, \omega) [f(v') f(v'_*) - f(v) f(v_*)] d\omega dv_*, \quad (1.2)$$

where ω is a unit vector on the sphere \mathbb{S}^{d_v-1} . The collision operator $Q(f, f)$ can also be rewritten as

$$Q(f, f)(v) = Q^+(f, f) + f Q^-(f), \quad (1.3)$$

where Q^+ denotes the gain term and Q^- is the loss term:

$$\begin{cases} Q^+(f, f) = \int_{\mathbb{R}^{d_v}} \int_{\mathbb{S}^{d_v-1}} \sigma(|v - v_1|, \omega) f(v') f(v'_*) d\omega dv_* \\ Q^-(f) = \int_{\mathbb{R}^{d_v}} \int_{\mathbb{S}^{d_v-1}} \sigma(|v - v_1|, \omega) f(v_*) d\omega dv_* \end{cases} \quad (1.4)$$

[☆]This work was partially supported by NSF grant DMS-1114546 and NSF DMS RNMS grant DMS-1107291 (KI-Net).

*Corresponding author. Tel: +86-21-34206383

Email addresses: mathvivi@sjtu.edu.cn (Wei Ren), hongliu@sjtu.edu.cn (Hong Liu), jin@math.wisc.edu (Shi Jin)

The velocity (v', v'_*) represent the post-collisional velocities whose relation to the pre-collisional velocities (v, v_*) are given by

$$\begin{cases} v' = \frac{1}{2}(v + v_* + |v - v_*|\omega), \\ v'_* = \frac{1}{2}(v + v_* - |v - v_*|\omega). \end{cases} \quad (1.5)$$

In Eqn. (1.2), σ is the nonnegative collision kernel which depends on the model of forces between particles, and we also define the total cross section σ_T as (see [5] for more details)

$$\sigma_T(|v - v_*|) = \int_{\mathbb{S}^{d_v-1}} \sigma(|v - v_*|, \omega) d\omega. \quad (1.6)$$

Meanwhile, one can refer to Chapman and Cowling [10] for the details of several models, such as the inverse power force model and the Lennard-Jones model. In the case of inverse k th power force between particles, it has the form

$$\sigma(|v - v_*|, \theta) = b_\alpha(\theta) |v - v_*|^\alpha, \quad (1.7)$$

where $\alpha = (k - 5) / (k - 1)$. In numerical simulation of rarefied gases, the variable hard sphere (VHS) model is often used, in which, $b_\alpha(\theta) = C_\alpha$, where C_α is a positive constant. The case $\alpha = 0$ corresponds to the Maxwellian gas, while the case $\alpha = 1$ represents the hard sphere gas.

With f , the macroscopic *density* ρ , *mean velocity* u , and *temperature* T , can be obtained by taking the moments:

$$\rho = \int_{\mathbb{R}^{d_v}} f dv, \quad u = \frac{1}{\rho} \int_{\mathbb{R}^{d_v}} v f dv, \quad T = \frac{1}{d_v \rho} \int_{\mathbb{R}^{d_v}} |v - u|^2 f dv. \quad (1.8)$$

Moreover, the collision operator (1.2) satisfies some important properties:

- Conservation laws:

$$\int_{\mathbb{R}^{d_v}} Q(f, f) \phi(v) dv = 0, \quad \text{for } \phi(v) = 1, v, |v|^2;$$

which gives conservation of mass, momentum and total energy.

- Boltzmann's H theorem [36]:

$$\frac{d}{dt} \int f \log f dv = \int Q(f, f) \log f dv \leq 0,$$

which implies that any system reaches its equilibrium state at which the entropy $-\int f \log f dv$ is maximum. The equilibrium distribution function has the form of a local Maxwellian distribution:

$$\mathcal{M}(\rho, u, T)(v) = \frac{\rho}{(2\pi T)^{d_v/2}} \exp\left(-\frac{|u - v|^2}{2T}\right). \quad (1.9)$$

The Knudsen number ε in (1.1), as a parameter of great significance in the kinetic theory, is the ratio of the local mean free path ℓ in gases to the characteristic length scale. For a small value of ε , the Chapman-Enskog expansion connects the Boltzmann equation (1.1) with hydrodynamic equations, i.e., the compressible Navier-Stokes equations (the first order approximation) and the compressible Euler equations (the zeroth order approximation). By taking $\varepsilon \rightarrow 0$, $f \rightarrow \mathcal{M}$, then one can obtain the hydrodynamic Euler equations

$$\begin{cases} \partial_t \rho + \nabla_x \cdot (\rho u) = 0, \\ \partial_t (\rho u) + \nabla_x \cdot (\rho u \otimes u + pI) = 0, \\ \partial_t E + \nabla_x \cdot [(E + p)u] = 0, \end{cases} \quad (1.10)$$

where E is the total energy, p is the pressure,

$$E = \frac{1}{2} \rho u^2 + \frac{d_v}{2} \rho T, \quad p = \rho T.$$

In addition, the heat flux q can be defined by

$$q = \frac{1}{2} \int_{\mathbb{R}^{d_v}} (v - u) [v - u]^2 f dv. \quad (1.11)$$

1.2. Computational difficulties: high-dimensions and stiffness

It is well accepted that the Boltzmann equation is valid for a wide range of ε , while the Navier-Stokes equations fail to reproduce accurate flowfields when ε is moderate or large [5, 9]. For example, in a typical space shuttle reentry problem, the mean free path ranges from 10^{-8} to $\mathcal{O}(1)$ meters, which means ε can vary from $\mathcal{O}(1)$ to a extremely small value. In this case, numerical methods for the Navier-Stokes equations are not suitable and at best can resolve the flowfields when $\varepsilon \ll 1$. Hence, numerically solving the Boltzmann equation becomes of great importance.

Basically, there are two main challenges in solving most kinetic problems numerically. The first is the high dimensions, and the second is multiple scales and numerical stiffness. For kinetic problems with high dimensions, it is evidential that the direct simulation Monte Carlo method (DSMC) is more efficient than the finite-difference methods [5]. Although conventional DSMC or other numerical methods are effective when the Knudsen number ε is large or moderate, the computational cost can be extremely expensive if ε vanishes. The reason is that numerical methods are generally required to *resolve* the small kinetic scale or time scale of $\mathcal{O}(\varepsilon)$, and it can be considerably time-consuming when $\varepsilon \rightarrow 0$. For a normal engineering problem, even running on clusters, it is common that one run of DSMC may take weeks or months.

In the past decades, a very promising numerical approach, the so-called *Asymptotic-Preserving schemes*, has been proposed and developed for kinetic equations efficient in the hydrodynamic regimes. The AP schemes allow a kinetic solver to capture the hydrodynamic behavior, as $\varepsilon \rightarrow 0$, without numerical resolving ε [16, 23, 24]. Specifically, as summarized by Jin [23], a scheme is AP if

- it preserves the discrete analogy of the Chapman-Enskog expansion;
- it computes the implicit collision terms explicitly, or more efficiently than an implicit solver based on Newton iterations.

A typical AP scheme uses either *implicit-explicit* (IMEX) time discretization or the exponential Runge-Kutta (ExpRK) method. In order to handle the implicit collision term efficiently, a BGK-penalization method was introduced by Filbet and Jin [16], utilizing the factor that the BGK collision operator

$$P(f) = \beta(M - f), \quad (1.12)$$

can be explicitly inverted. As a result, one can obtain a Boltzmann solver uniformly stable with respect to ε , and yet can be implemented explicitly. Later, Yan and Jin [39] proposed a *successive penalty* AP scheme which was positivity-preserving and has strong AP properties. Their method had been implemented in the finite difference framework in [39].

Earlier, Pareschi and Caflisch [31] formulated a hybrid Monte Carlo method that performed well in the fluid dynamic regime for the space homogeneous Boltzmann equation. The method was based on an analytic representation of the solution and implicit time differencing derived from a generalized Wild expansion [17, 37]. Meanwhile, Pareschi and Russo [32] introduced the *Time-Relaxed* schemes, which was a linear penalty method with $P(f) = \beta f$, and the schemes absorbed the stiff part into the time derivative $\partial_t f$ to remove the stiffness. Using the bilinearity of the remaining term $\tilde{Q}(f, f) = Q(f, f) + \beta f$, the distribution function can be represented by finite terms in the Wild Sum [17, 37]. It was reported that higher order accuracy in time can be achieved by keeping more expansion terms were kept. Then Pareschi and Trazzi [33] extended this class of AP schemes to two dimensions in space, and demonstrated its better performance in efficiency compared with the conventional DSMC method as $\varepsilon \rightarrow 0$. Later, Degond et al. [12] introduced a *moment-guided Monte Carlo* method to reduce the variance. They solved the kinetic equation and the fluid equations respectively, and matched the moments of both solutions. Preliminary numerical results showed reductions of fluctuations in all regimes compared to DSMC. Recently, DiMarco and Pareschi [13] demonstrated that the Maxwellian truncation criterion used in [17] was equivalent to the Filbet-Jin BGK penalization for space homogeneous case.

An alternative construction of AP schemes was proposed by DiMarco and Pareschi [13]. The methods were based on a decomposition of the collision operator into an equilibrium and a nonequilibrium part, and then the stiff part was absorbed in an *explicit Runge-Kutta* (ExpRK) framework. Recently, Li and Pareschi [29] introduced more sophisticated ExpRK methods for the full Boltzmann equation, which were deterministic methods. It was presented in their work [29] that higher order time discretization methods performed better in numerical tests due to their higher

order accuracy. One should note that in their methods WENO schemes were applied to ensure sufficiently high-order accuracy in space, while in the particle-based algorithms mentioned above, such as DSMC and TRMC (a Monte Carlo implementation of the time relaxed schemes), applying high-order space discretization methods was extremely limited in space non-homogeneous cases.

The goal of this work is to propose a new *asymptotic-preserving direct simulation Monte Carlo method* (AP-DSMC) based on the successive penalty AP time-discretization [39]. This line of research is of significance not only in rarefied gas and reentry problems [22, 26, 27, 30, 38] governed by the Boltzmann equation, but also in some more complicated transport phenomena, whose master equations are the quantum Boltzmann equation [15] and the Landau equation [25] in plasma physics. For the space homogeneous Boltzmann equation, it was realized in [39] that the successive penalization step can be written as a convex combination of the density distribution of the previous time step, a positive collision operator and the local Maxwellian. This forms the basis for a Monte-Carlo implementation [31]. Since the coefficients of this convex combination are all positive, for any time step, this method has a numerical stability (as well as the number of sampling particles) independent of the Knudsen number, thus is much more efficient than the conventional DSMC methods. This is highly desirable for the reentry problems and any other kinetic problems that involve multiple time and spatial scales. Some of the theoretical properties of this scheme, such as positivity and asymptotic-preservation, are also explored.

We also compare this method with some other asymptotic-preserving Monte-Carlo methods, including the time-relaxed Monte-Carlo [32] (TRMC) and the exponential Monte-Carlo method [13] (denoted as ExpRK in the following). Our numerical experiments indicate that they give comparable results for most regimes, except the heat flux for moderately small ε . Thus the focus will be the computational cost. Their computational cost varies depending on the coefficients in the aforementioned convex combination. Since the AP-DSMC method proposed in this paper puts less weight on the most expensive Maxwellian sampling, it is computationally more efficient in the intermediate regime where the time step is of the order of mean free path. In addition, with under-resolved solutions, especially considering the values of heat flux, results by AP-DSMC agree with the reference solutions better than ExpRK, which can be attributed to the ability of reproducing more accurate distribution functions with AP-DSMC in the intermediate regime.

The rest of the paper is organized as follows. In section 2, we briefly review the two existing Monte Carlo methods with asymptotic preserving properties for the Boltzmann equation. In section 3 we introduce the new AP-DSMC based on the successive penalty method in the first order formulations and study the properties and computational efficiency of this method as well as ExpRK and TRMC. Finally in section 4, several numerical results for the new AP-DSMC are presented which show the good performance in capturing the macroscopic behavior in various flow regimes. Several other methods are compared in efficiency and capability of capturing unsteady profiles. Some simple physical problems involving real gas are computed here to demonstrate the capability of our new methods in engineering applications. The paper is concluded in section 5.

2. Some asymptotic preserving Monte Carlo methods for the Boltzmann equation

In this section, two existing asymptotic preserving Monte Carlo methods are briefly described, which will be used to compare with the new method proposed in this paper.

2.1. The TRMC methods

Pareschi and Russo [32] derived the time-relaxed Monte Carlo methods based on the time-relaxed approach proposed in [17] that utilized the Wild Sum [37]. Briefly speaking, letting $F(\tau, \nu) = f e^{\beta t/\varepsilon}$ and $\tau = 1 - e^{-\beta t/\varepsilon}$, the homogeneous Boltzmann equation in general with a linear penalty term $\beta f/\varepsilon$ can be rewritten into

$$\begin{cases} \frac{\partial F}{\partial \tau} = \frac{1}{\beta} \tilde{Q}(F, F), \\ F(\tau = 0, \nu) = f_0, \end{cases} \quad (2.1)$$

where for a general distribution function f , we define

$$\tilde{Q}(f, f) = Q(f, f) + \beta f, \quad (2.2)$$

and the positive constant β is an upper bound of the coefficient of the loss term Q^- in (1.4):

$$\beta \geq Q^-. \quad (2.3)$$

Then the solution to problem (2.1) using the *Wild Sum* can be truncated to yield the following method:

$$f^{n+1} = \sum_{p=0}^m a_p f_p + a_{m+1} \mathcal{M}, \quad m \geq 1, \quad (2.4)$$

where the functions f_p are given by the recurrence formula

$$f_{p+1} = \frac{1}{p+1} \sum_{h=0}^p \frac{1}{\beta} \tilde{Q}(f_h, f_{p-h}), \quad p = 0, 1, \dots \quad (2.5)$$

Take the so-called *first order TRMC* (*TRMC1*) as an example, one can use $a_0 = 1 - \tau$, $a_2 = \tau^3$, and $a_1 = 1 - a_0 - a_2$. We refer to Pareschi and Russo [32], Pareschi and Trazzi [33] for more details. In this paper, both ExpRK method and this method are used to compare with our new AP-DSMC.

Remark 2.1. Note that, according to [32, 33], by including more terms in (2.4), one can get a more time accurate approximate distribution function for the homogeneous Boltzmann equation (2.1). Here we just give an example called *TRMC2*, which is second order accurate in time:

$$f^{n+1} = a_0 f^n + a_1 f_1 + a_2 f_2 + a_3 \mathcal{M}, \quad (2.6)$$

where $a_0 = 1 - \tau$, $a_1 = \tau(1 - \tau)$, $a_3 = \tau^4$ and $a_2 = 1 - a_0 - a_1 - a_3$, with

$$f_1 = \frac{\tilde{Q}(f^n, f^n)}{\beta}, \quad f_2 = \frac{\tilde{Q}(f^n, f_1)}{\beta}.$$

The formulation (2.6) of *TRMC2* is similar to *TRMC1* except f_2 . According to [32], the probabilistic interpretation of f_2 is that a group of particles sampled from f^n undergo dummy collisions with another group of particles sampled from f_1 . It is reported [33] that *TRMC2* needs more computational time than *TRMC1* with the same numerical setup. In addition, Pareschi and Russo [32] gave the positivity proof of the *TRMC* methods.

2.2. The ExpRK method

Secondly, we briefly review the explicit exponential Runge-Kutta methods [13]. Still, we present the treatment on the homogeneous Boltzmann equation here. The basic idea is

1. Penalize Q by P (Eqn. (1.12));

$$\frac{\partial f}{\partial t} = \frac{1}{\varepsilon} (\tilde{Q}(f, f) - \beta \mathcal{M}) + \frac{\beta}{\varepsilon} (\mathcal{M} - f), \quad (2.7)$$

2. Absorb the stiff part into the time derivative term;

$$\frac{\partial [(f - \mathcal{M}) e^{\beta t/\varepsilon}]}{\partial t} = \left[\frac{1}{\varepsilon} (\tilde{Q}(f, f) - \beta \mathcal{M}) - \partial_t \mathcal{M} \right] e^{\beta t/\varepsilon}. \quad (2.8)$$

3. Solve the scheme with an *explicit Runge-Kutta* method, using $M^{n+1} = M^n$ (due to the conservation of the moments for space homogeneous Boltzmann equation); (i.e. explicit Euler method)

$$\begin{aligned} f^{n+1} &= \mathcal{M}^n + a \left[f^n - \mathcal{M}^n + \mu \left(\frac{\tilde{Q}(f^n, f^n)}{\beta} - \mathcal{M}^n \right) \right] \\ &= a f^n + \mu a \frac{\tilde{Q}(f^n, f^n)}{\beta} + [1 - (1 + \mu) a] \mathcal{M}^n. \end{aligned} \quad (2.9)$$

where $a = e^{-\beta \Delta t/\varepsilon}$, with

$$\mu = \frac{\beta \Delta t}{\varepsilon}, \quad (2.10)$$

and the term \mathcal{M}^n can be computed by Pullin's method [34].

The positivity of f^{n+1} is guaranteed since both M^n and $\tilde{Q}(f^n, f^n)$ are positive by their definitions: (1.9) and (2.2) respectively. One can also refer to [13, 29] for more details.

Remark 2.2. *Pullin's method can be described as follows:*

1. Compute the momentum $m\bar{u}$ and the energy E' of N related particles;

$$m\bar{u} = \frac{1}{N} \sum_{i=1}^N mu_i, \quad E' = \sum_{i=1}^N \left[e_i + \frac{1}{2} m |u_i - \bar{u}|^2 \right], \quad (2.11)$$

where u_i is the velocity for the i -th particle, e_i denotes internal energy, $\sum_{i=1}^N e_i = \frac{\sum_{i=1}^N \vartheta_i}{2} RT$, where $\vartheta_i = 0$ for monatomic gas particles, and $\vartheta_i = 2$ for diatomic gas particles. Here e_i is not considered in this work, and E' is the total mass center energy of all particles.

2. Sample same number of particles from a Maxwellian distribution with the same momentum $m\bar{u}$ and energy E' ;
3. Replace the original particles with the sampled ones.

Note that the artificial diffusion nature of Pullin's method was reported in [7] and [30].

3. A generalized AP-DSMC scheme and its properties

In this section, a general form of the AP-DSMC scheme is introduced and the corresponding properties are discussed. This method is based on the work of Yan-Jin [39], which is an improvement of the original Filbet-Jin BGK penalization method [16]. We choose one of these methods as our new AP-DSMC and give its computational procedures.

3.1. The successive penalty method for Monte Carlo computations

3.1.1. Time splitting of the full Boltzmann equation

Here, a simple time splitting scheme is applied to Eqn. (1.1) and then we have

$$\begin{cases} \frac{\partial f}{\partial t} + v \cdot \nabla_x f = 0, \\ \frac{\partial f}{\partial t} = \frac{1}{\varepsilon} Q(f, f), \end{cases} \quad (3.1)$$

which consists of solving the first transport equation for one time step to generate the initial data for the collision step for one time step. Here, we discretize the transport equation in time by the forward Euler method:

$$\frac{f^* - f^n}{\Delta t} = -v \cdot \nabla_x f^n. \quad (3.2)$$

Since the numerical difficulties are mainly within the collision step, or the space homogeneous equation here, we spend most of efforts on this part in the sequel.

3.1.2. The BGK-penalization in the space homogeneous equation

With the BGK penalization term $P(f) = \beta(\mathcal{M} - f)$, where β is defined in (2.3), one writes

$$\frac{\partial f}{\partial t} = \underbrace{\frac{1}{\varepsilon} (Q(f, f) - P(f))}_{\text{less stiff}} + \underbrace{\frac{1}{\varepsilon} P(f)}_{\text{stiff}}. \quad (3.3)$$

As discussed in [16, 39], the first term on the right hand side (RHS) is less stiff and the second one contains more stiffness. Again, we apply the time splitting for simplicity:

$$\begin{cases} \frac{\partial f}{\partial t} = \frac{1}{\varepsilon} (Q(f, f) - P(f)), \\ \frac{\partial f}{\partial t} = \frac{1}{\varepsilon} P(f), \end{cases} \quad (3.4)$$

where the first equation is solved explicitly, to get

$$\frac{f^{**} - f^*}{\Delta t} = \frac{1}{\varepsilon} (Q(f^*, f^*) - P(f^*)). \quad (3.5)$$

The same time discretization as [39] is used here for the equation with more stiff term and we divide the time step into L subintervals. Then

$$\begin{cases} \frac{f^{n+1,1} - f^{**}}{\Delta t/L} = \frac{1}{\varepsilon} P^{n+1,1}, \\ \frac{f^{n+1,2} - f^{n+1,1}}{\Delta t/L} = \frac{1}{\varepsilon} P^{n+1,2}, \\ \dots \\ \frac{f^{n+1} - f^{n+1,L-1}}{\Delta t/L} = \frac{1}{\varepsilon} P^{n+1}. \end{cases} \quad (3.6)$$

Due to the conservation property of operator P , we have $\mathcal{M}^{n+1,1} = \mathcal{M}^{n+1,2} = \dots = \mathcal{M}^{n+1} = \mathcal{M}^{**}$, then (3.6) can be rewritten as

$$\begin{cases} f^{n+1,1} = c f^{**} + (1-c) \mathcal{M}^{**}, \\ f^{n+1,2} = c f^{n+1,1} + (1-c) \mathcal{M}^{**}, \\ \dots \\ f^{n+1} = c f^{n+1,L-1} + (1-c) \mathcal{M}^{**}, \end{cases} \quad (3.7)$$

where

$$c = \left(1 + \frac{\beta \Delta t}{\varepsilon L}\right)^{-1}. \quad (3.8)$$

One can obtain a general formula for any $L \in \mathbb{Z}^+$ as follows:

$$f^{n+1} = c^L f^{**} + (1 - c^L) \mathcal{M}^{**}. \quad (3.9)$$

This splitting is referred as SP_L .

Furthermore, since $\mathcal{M}^{**} = \mathcal{M}^*$, so when $L = 2$, this split version can be rewritten into a much more clear and unified form

$$\begin{cases} f^* = f^n - \nu \Delta t \cdot \nabla_x f^n, \\ f^{n+1} = \mathcal{M}^* + c_1 \cdot \left[(f^* - \mathcal{M}^*) + c_2 \cdot \left(\tilde{Q}(f^*, f^*) / \beta^* - \mathcal{M}^* \right) \right], \end{cases} \quad (3.10)$$

where the coefficients $c_1 = c^L (= (1 + \mu/2)^{-2}$ for $L = 2$), $c_2 = \mu$. For $L > 2$ cases, one can obtain the similar form as (3.10) with different value of c in (3.8).

Moreover, (3.10) can be further reformulated as

$$\begin{cases} f^* = \underbrace{f^n}_{\text{original distribution}} + \underbrace{\nu \Delta t \cdot (-\nabla_x f^n)}_{\text{transport}}, \\ f^{n+1} = \underbrace{b_0 f^*}_{\text{not colliding}} + \underbrace{b_1 \tilde{Q}(f^*, f^*) / \beta^*}_{\text{colliding}} + \underbrace{b_2 \mathcal{M}^*}_{\text{relaxation}}. \end{cases} \quad (3.11)$$

Note that the term $\tilde{Q}(f^*, f^*)/\beta^*$, according to the definition of \tilde{Q} in Eqn. (2.2), can be regarded as a distribution function [32], and can be approximated by the Nanbu-Babovsky's method [3]. Besides, in Eqn. (3.11), the *weights* are defined as

$$\begin{cases} b_0 = c_1, \\ b_1 = c_1 c_2, \\ b_2 = 1 - c_1 - c_1 c_2. \end{cases}$$

Therefore the computational procedure can be summarized as:

1. Compute f^* from transport;
2. Compute the weights b_0 , b_1 , and b_2 ;
3. Compute the collision term \tilde{Q}^*/β^* with the prescribed collisional law;
4. Compute the relaxation term \mathcal{M}^* with the method introduced by Pullin [34] (See Remark 2.2);
5. Sample f^{n+1} from the no-colliding part, colliding part and relaxation part by corresponding probability b_0 , b_1 and b_2 respectively.

Remark 3.1. As mentioned in Eqn. (2.3), β is a positive constant. Numerically, it is considered as a variable and updated at each time step (i.e. β^n at the n -th time step) if necessary in order to obtain a better estimation of β [15].

3.2. Procedures of the new AP-DSMC scheme

Below we give details of the AP-DSMC algorithm.

3.2.1. Initialization

First of all, a finite number of simulation particles is employed in the AP-DSMC to represent the N -particle ($N \rightarrow \infty$) system governed by the Boltzmann equation, and the distribution function f is approximated by a sufficiently large number of samples in our new scheme. In general, the *weight factor* $w_p \in \mathbb{Z}$ indicates that w_p real molecules are represented by one simulation particle. The computational domain is often divided into a great number of cells $\{m = 1, \dots, MNC\}$, where MNC is the total number of cells, to locate particles and sample the local macroscopic quantities. Given the initial condition (ρ , v and T) in cell m , one can obtain the number of particles N_m by

$$N_m = \lfloor \frac{\rho V_m}{w_p} \rfloor, \quad (3.12)$$

here $\lfloor x \rfloor$ is the largest integer which is less than or equal to x , and V_m is the volume of cell m . Then, the local Maxwellian distribution function $\mathcal{M}(v, T)$ is applied to generate N_m particles and their initial velocities,

$$\{v_{i,j}^n, i = 1, \dots, N, j = 1, \dots, d_v\}.$$

As a matter of fact, any prescribed distribution function g is allowed to generate particles on the condition that g can be analytically represented. Since our simulations are particle-based, the dimensionless macroscopic quantities are computed by the corresponding particles information, which is similar to that in [5]:

$$\rho = \frac{N_m w_p}{V_m}, \quad u_j = \frac{1}{N_m} \sum_{i=1}^{N_m} v_{i,j}, \quad d_v T = \frac{1}{N_m} \left(\sum_{i=1}^{N_m} \sum_{j=1}^{d_v} v_{i,j}^2 - N_m \sum_{j=1}^{d_v} u_j^2 \right). \quad (3.13)$$

3.2.2. Convection

Transport all the particles by their velocity v_i^n for one time step Δt :

$$x_i^{n+1} = x_i^n + v_i^n \cdot \Delta t. \quad (3.14)$$

Relocate the transported particles by sorting all the particles to cells according to their positions, especially for a Cartesian mesh. For example, for the 1D i -th cell, the two cell edge positions of this cell are pos_i and pos_{i+1} , and then an arbitrary j -th particle can be considered locating in this cell if

$$pos_i < x_j < pos_{i+1}. \quad (3.15)$$

3.2.3. Collision

The details of the computation of the collision part can be described as follows:

Algorithm 1. (First order AP-DSMC)

1. do $n = 1, n_{tot}$
 - compute an upper bound σ_{\max} of the cross section
 - select a random pair (i, j) uniformly in N_c^n
 - compute the relative cross section σ_{ij}
 - if $\sigma_{\max} \cdot \xi < \sigma_{ij}$ (called the acceptance-rejection method)
 - perform the collision and compute the post-collisional velocities according to the collisional law
 - let $v_i^{n+1} = v'_i$, and $v_j^{n+1} = v'_j$
 - select N_M^n particles among those that have not been selected, and compute the overall momentum and energy
 - replace those N_M^n selected the same number of particles by sampling from the Maxwellian with the same momentum and energy
 - set $v_i^{n+1} = v_i^n$ for all the particles that have not collided
- end do

Here $\sigma_{ij} = \sigma_T (|v_i - v_j|)$, $\sigma_{\max} = \max\{\sigma_{ij}\}$, and β can be chosen as $\rho\sigma_{\max}$. ξ is a random number uniformly in $[0, 1]$. At the n -th step, N^n is the number of particles, N_c^n is the number of collision pairs to select, and N_M^n is the number of particles to be replaced with that sampled from the Maxwellian with the same momentum and energy:

$$N_c^n = \begin{cases} \lfloor b_1 N^n / 2 \rfloor, & t^n = 0, \\ \lfloor b_1 N^n / 2 + \chi_{N_c}^{n-1} \rfloor, & t^n = n \cdot \Delta t, \end{cases} \quad \text{and} \quad N_M^n = \begin{cases} \lfloor b_2 N^n / 2 \rfloor, & t^n = 0, \\ \lfloor b_2 N^n / 2 + \chi_{N_M}^{n-1} \rfloor, & t^n = n \cdot \Delta t, \end{cases}$$

where Δt denotes the time increment, $\chi_x^{n-1} = x^{n-1} - \lfloor x^{n-1} \rfloor$ computed in the previous time step t^{n-1} .

Remark 3.2. For a typical DSMC method, the error depends on the following parameters:

1. Space and time discretizations, Δx and Δt ;
2. The number of particles, N ;
3. The number of samples with Monte Carlo methods, N_s .

The errors can be classified into two kinds: one is the truncation error due to the spatial [1, 20] and temporal [18] discretizations; the other one is the statistical error which can be attributed to the finite number of samples, which depends on $N \cdot N_s$. One can refer to the exclusive references [11, 21] for further discussions on the statistical error in DSMC.

3.3. Properties of the AP-DSMC scheme

3.3.1. Positivity preserving

For the direct simulation Monte Carlo simulation, the property of positivity preserving is required. In Eqn. (3.11), assuming the weights are nonnegative, three terms need the proof of positivity preserving:

1. transport term, $(f^n + v\Delta t \cdot (-\nabla_x f^n))$;
2. colliding term, $\tilde{Q}(f^*, f^*) / \beta^*$;
3. relaxation term, \mathcal{M}^* .

Define the CFL condition as

$$\Delta t \leq \Delta x / u_{\max}, \quad (3.16)$$

where Δx is the local mesh size (or space step) and u_{\max} is the truncation of the velocity domain. With a suitably chosen spatial discretization for $\nabla_x f$ (for example the upwind scheme), the transport term is positive if the CFL condition (3.16) is satisfied.

As defined in Eqn. (2.2), we have

$$\begin{aligned} \tilde{Q} &= Q + \beta f \\ &= Q^+ + f(\beta - Q^-), \end{aligned}$$

where Q^+ is the gain term defined in (1.4) and is positive. With the condition (2.3), $\beta - Q^- \geq 0$. Hence, \tilde{Q} is positive and then the colliding term $\tilde{Q}(f^*, f^*)/\beta^*$ in (3.11) is positive. As for the relaxation term, it is obvious that \mathcal{M}^* is positive according to its definition Eqn. (1.9).

Therefore, having nonnegative weights b_i and a nonnegative initial distribution, our scheme AP-DSMC can preserve the positivity during the whole computation.

3.3.2. Asymptotic preserving property

The scheme defined in Eqn. (3.11) is conservative and asymptotic preserving when the nonnegative weights b_i ($0 < c \leq 1$ in (3.8), then $b_i \geq 0$) satisfy the following conditions:

1. Conservation.

$$\sum_{i=0}^2 b_i = 1. \quad (3.17)$$

2. Asymptotic preservation (AP).

$$\lim_{\mu \rightarrow \infty} b_0 = 0, \quad \lim_{\mu \rightarrow \infty} b_1 = 0. \quad (3.18)$$

Name the scheme as SP_L once L in (3.9) is given. It can be deduced that SP_1 can not be considered as an AP scheme since $\lim_{\mu \rightarrow \infty} b_1 = 1$, which does not satisfy the condition (3.18). Meanwhile, it was shown in [39] that for $L \geq 2$, SP_L is AP in the sense that

$$f^n - \mathcal{M}^n = \mathcal{O}(\varepsilon), \text{ for any } n \geq 1. \quad (3.19)$$

3.3.3. Estimation of the computational efforts

In a typical DSMC method, the total number of collision pairs N_t during one time step Δt and the collision frequency ν given by kinetic theory [5, 6]:

$$N_t = \frac{1}{2} N \nu \Delta t, \quad (3.20)$$

where the collision frequency is

$$\nu = \frac{1}{\varepsilon} \rho \overline{\sigma_T}. \quad (3.21)$$

Here, with (1.6), $\overline{\sigma_T}$ is given by

$$\overline{\sigma_T} = \frac{1}{\rho^2} \int_{\mathbb{R}^{d_v}} \sigma_T (|v - v_*|) f(v) f(v_*) dv_*. \quad (3.22)$$

Two aspects should be clarified here: one is the computation of $\overline{\sigma_T}$, and the other is the estimation of the computational efforts. As a matter of fact, instead of direct calculation of $\overline{\sigma_T}$, which is time consuming, several schemes have been developed to reproduce the actual mean collision rate [5, 6]. Here, we choose two typical schemes, Bird's no time counter (NTC) scheme and Nanbu-Babovsky's scheme, to unfold the discussion.

- **NTC scheme.** In this scheme, the computation is driven (or proceeds) to the next time step when the required number of dummy collision pairs N_c is selected. The selected pairs will be conducting examinations with the acceptance-rejection method to make sure if the binary collisions happen. Here

$$N_c = \frac{1}{2} N \rho \sigma_{\max} \Delta t / \varepsilon,$$

and the probability of each intermolecular collision between the i -th particle and the j -th particle is $P = \frac{\sigma_{i,j}}{\sigma_{\max}}$, where $\sigma_{\max} = \max\{\sigma_{ij}\}$ is the maximum collision cross section. Hence, after conducting a sufficient number of collisions, the value of $\overline{\sigma_T}$ can be reproduced;

- **Nanbu-Babovsky's scheme.** Usually, for the collision equation (the second equation in (3.11)), the time step Δt is divided into several subintervals (i.e. L_t) in order to ensure that each particle is selected as one of a dummy collision pair at most once, while the transport equation (the first equation in (3.11)) still proceeds with Δt . Here,

$$\Delta t_c = \frac{\Delta t}{L_t} < \frac{1}{\nu}, \text{ or } N_c < \frac{N}{2} \quad (3.23)$$

should be satisfied so that the required number of dummy collision pairs N_c will not exceed the actual number of $N/2$ pairs during the time subintervals Δt_c . Given a time step Δt for the computation, one can choose an appropriate L_t :

$$L_t > \frac{\rho \sigma_{\max} \Delta t}{\varepsilon}.$$

The rest of procedures is same as the NTC scheme.

- **AP-DSMC.** Our new scheme is driven to the next time step after all particles are dealt with during each time step Δt . By the definition (3.11), one should treat the particles, as classified into three groups, in three different ways:
 1. no-colliding particles, $\lfloor b_0 N \rfloor$: keep the velocity of particles unchanged to the next time step;
 2. colliding particles, $\lfloor b_1 N \rfloor$: select $\lfloor \frac{1}{2} b_1 N \rfloor$ dummy collision pairs and conduct the collision examinations with the acceptance-rejection (See Algorithm 1);
 3. relaxation particles, $\lfloor b_2 N \rfloor$: replace them with new particles sampled from the corresponding Maxwellian distribution preserving the number, momentum and energy conservations.

Note that since $b_1 < 1$, which is satisfied *unconditionally*, the constraint (3.23) on the time step for the collision equation is unnecessary in this scheme.

Numerically speaking, as the particle-based algorithms, the computational costs of the collision treatments of both Bird's NTC scheme and Nanbu-Babovsky's scheme are proportional to N_t , while the cost of AP-DSMC is proportional to $(b_1/2 + b_2) N$. In order to compare the difference of the above three schemes in computational efforts for $\varepsilon \rightarrow 0$ (or in the hydrodynamic limit), we fixed the values of $\rho \sigma_{\max} \Delta t$ and N . Then, for conventional DSMC methods,

$$N_t \propto \varepsilon^{-1},$$

while for AP-DSMC, the value of $(b_1/2 + b_2)$ is bounded by 1 despite of the dependence of b_i on ε . Hence, it can be deduced that AP schemes will be much more efficient than conventional DSMC methods when ε is vanishing.

3.3.4. Main differences among the AP-DSMC schemes

Our numerical experiments in section 4 indicate that these methods give comparable numerical results in most cases, except heat flux for moderately small ε . Thus the main issue here will be the computational cost. Since all schemes under consideration can be put in the form of (3.11) with different coefficients (see Table 3.1), one should first compare the cost of computing the collision term \hat{Q}/β and the local Maxwellian \mathcal{M}^* .

To this aim, we conduct a test on a regular laptop with the current Monte Carlo code. The same code is used with different weights:

Table 3.1: Coefficients in several AP methods. (μ is defined in (2.10))

| Name | b_0 | b_1 | b_2 |
|-----------------|--------------------|--|---------------------------------|
| SP ₁ | $(1 + \mu)^{-1}$ | $\mu(1 + \mu)^{-1}$ | 0 |
| SP ₂ | $(1 + \mu/2)^{-2}$ | $\mu(1 + \mu/2)^{-2}$ | $1 - (1 + \mu)(1 + \mu/2)^{-2}$ |
| SP ₃ | $(1 + \mu/3)^{-3}$ | $\mu(1 + \mu/3)^{-3}$ | $1 - (1 + \mu)(1 + \mu/3)^{-3}$ |
| ExpRK | $e^{-\mu}$ | $\mu e^{-\mu}$ | $1 - (1 + \mu)e^{-\mu}$ |
| TRMC1 | $e^{-\mu}$ | $(1 - e^{-\mu})(2 - e^{-\mu})e^{-\mu}$ | $(1 - e^{-\mu})^3$ |

- RUN-M: letting $b_2 = 1$ and $b_0 = b_1 = 0$ to conduct sampling \mathcal{M} only;
- RUN-Q: setting $b_1 = 1$ and $b_0 = b_2 = 0$ to sample \tilde{Q}/β only

The other numerical setups are specified as follows. The simulations are initialized with $(\rho, \nu, T) = (1, 0, 1)$ and 50 particles in only one cell. Particle transportation and boundary conditions are not considered, and all particles are forced to be involved in collision pairs selection. The computational time for RUN-M is $t_1 = 4 \times 10^{-7}s$, and for RUN-Q is $t_2 = 9.36 \times 10^{-8}s$. Then $t_1/t_2 \approx 4.33$. With a larger number of particles, it is found that the ratio t_1/t_2 increases, i.e. about 5.0 for 10^3 particles per cell, and when the number of particles per cell decreases to 10, the ratio t_1/t_2 is about 4.0. Hence, it can be noticed that sampling \mathcal{M} is more time-consuming in typical simulations, therefore one should minimize b_2 for all μ to save the computational cost, when other conditions in (3.17) and (3.18) are met. Note for SP_L,

$$b_2 = 1 - b_0 - b_1 = 1 - b_0 - \mu b_0 = 1 - b_0(1 + \mu),$$

thus one should maximize $b_0 = (1 + \mu/L)^{-L}$, namely, choose L such that

$$\begin{aligned} L_0 &= \operatorname{argmin}_f(x, L), \\ &= \operatorname{argmin} \left[(1 + x/L)^{-L} \right], \text{ for } \forall x \in \mathbb{R}^+. \end{aligned} \quad (3.24)$$

Since $(1 + x/L)^{-L}$ is monotonically increasing in L for any $x \in \mathbb{R}^+$, L_0 in Eqn. (3.24) should be the smallest value of its range to achieve the minimum. Clearly, $L_0 = 2$ (corresponding to SP₂) should be the *optimal one in our class of AP schemes* in the viewpoint of computational efficiency, since the scheme with $L_0 = 1$ (which refers to SP₁) is eliminated above.

Considering when the difference between the two values of b_0 occurs, a new indicator $\Theta(\mu)$ is defined in this paper. Taking the comparison SP_L with ExpRK as an example, we have:

$$\Theta(\mu) = (1 + \mu/L)^{-L} - e^{-\mu}, \quad \mu \in \mathbb{R}^+. \quad (3.25)$$

Obviously, $\Theta(\mu)$ is always positive. Fig. 1 plots the tendency of $\Theta(\mu)$ with μ varying, and noticeable peaks are observed in the region $x \in [10^0, 10^1]$ for both $L = 2$ and $L = 3$.

From the viewpoint of efficiency, for the hydrodynamic limit, all the AP schemes reduce to a Euler solver ($b_0 = b_1 = 0$) and cost the same computational efforts. For near-continuum regime simulations, however, b_0 is usually non-trivial, and then the difference in computational efficiency for various AP schemes can be noticed. As a matter of fact, it can be deduced from Fig. 1 that if in the regime $\varepsilon \ll 1$, $\Delta t = \mathcal{O}(\varepsilon)$, SP₂ is more efficient than SP₃, and SP₃ can save more cost than ExpRK. Note that the peak in Fig. 1 is not exact value of the difference in computational time. It is just a qualitative demonstration. For simplicity, we name SP₂ as AP-DSMC in the following.

Remark 3.3. *It should be noticed that Fig. 1 only indicates when the difference between AP-DSMC and ExpRK occurs, while the exact scale of difference is case dependent. In the following, it is evidential that for some cases the difference between the two AP schemes can be over 20%.*

4. Numerical simulations

In this section, six numerical tests are conducted in order to

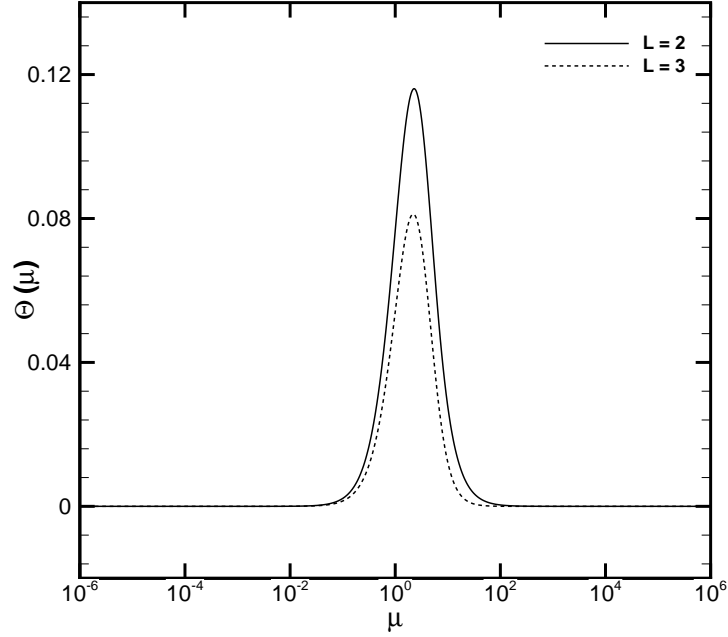


Figure 1: $\Theta(\mu)$ with varying μ plots for both $L = 2$ (solid lines) and $L = 3$ (dash lines).

- test the AP-DSMC scheme and others.
- validate our code with the DSMC method [5] and second order Filbet-Jin method [16].
- define the differences among AP-DSMC and ExpRK in both efficiency and accuracy.
- prove the capability of our scheme in higher dimensional applications, i.e. 2D transient flows.

For all Filbet-Jin solutions, $N_\nu = 32$ mesh points are uniformly distributed in each ν direction with $v_{\max} = 8$ and $v_{\min} = -8$. Meanwhile, the van Leer type slope limiter [28] is applied on the computation of the transport step, and $\Delta t = \frac{\Delta x}{2v_{\max}}$ ($CFL = 0.5$) is taken to guarantee the stability.

Note that in numerical test 1 to 3, the maximum collision rate σ_{\max} is chosen to be 1.0 so as to compare with the results from the deterministic methods or conventional DSMC methods, while in numerical test 4 to 6, the comparisons are conducted with other DSMC methods and σ_{\max} is updated at each time step if it increases.

4.1. Numerical Test 1: Statistical error test

At first, we report on the results of a stochastic error analysis with respect to the number of particles N .

4.1.1. The initial data

The initial data is a non-equilibrium distribution

$$f^0(x, \nu) = \frac{\rho^0(x)}{2\pi T^0(x)} \frac{1}{2} \left\{ \exp\left(-\frac{|\nu - u^0(x)|^2}{2T^0(x)}\right) + \exp\left(-\frac{|\nu + u^0(x)|^2}{2T^0(x)}\right) \right\} \quad (4.1)$$

where

$$\begin{cases} \rho^0(x) = \frac{2 + \sin(2\pi x)}{3}, \\ u^0(x) = \begin{pmatrix} \frac{1}{5} \cos(2\pi x) \\ 0 \end{pmatrix}, \\ T^0(x) = \frac{3 + \cos(2\pi x)}{4}. \end{cases} \quad (4.2)$$

To obtain the initial distribution in AP-DSMC, one can regard $f^0(x, v)$ as the linear combination of two distribution functions $\frac{1}{2}f_1^0(x, v)$ and $\frac{1}{2}f_2^0(x, v)$, where

$$f_1^0(x, v) = \frac{\rho^0(x)}{2\pi T^0(x)} \cdot \exp\left(-\frac{|v - u^0(x)|^2}{2T^0(x)}\right), \quad f_2^0(x, v) = \frac{\rho^0(x)}{2\pi T^0(x)} \cdot \exp\left(-\frac{|v + u^0(x)|^2}{2T^0(x)}\right).$$

Obviously, both f_1^0 and f_2^0 can be realized by sampling from Maxwellian distribution functions. Hence, in the procedure of direct simulations, one can sample the initial condition (4.1) by the following three steps:

1. sample f_1^0 from $\mathcal{M}(\rho^0, u^0, T^0)$;
2. sample f_2^0 from $\mathcal{M}(\rho^0, -u^0, T^0)$;
3. sum up: $f^0 = \frac{1}{2}f_1^0 + \frac{1}{2}f_2^0$.

In this test, the periodic boundary conditions at both ends of the computational domain are applied. In addition, cases at $\varepsilon = 1, 10^{-3}, 10^{-6}$ are computed respectively, and the output time is 0.05 with $\sigma_{\max} = 1.0$, $\Delta x = 10^{-2}$ and $\Delta t = 10^{-3}$. The reference solutions are computed by the Filbet-Jin method with $\Delta x = 10^{-2}$ and $\Delta t = 6.25 \times 10^{-4}$.

4.1.2. The convergence rate

In order to measure the errors from N to investigate the stochastic nature of the method, a L_2 norm are defined [12] by:

$$E_2(N) = \sqrt{\frac{1}{N_s} \sum_{i=1}^{N_s} \sum_{j=1}^{N_x} (\Phi_{i,j}(N) - \bar{\Phi}_j)^2}, \quad (4.3)$$

where $\Phi_{i,j}$ is the solutions computed at cell j and for the i -th run, $\bar{\Phi}_j$ is the reference solutions from the Filbet-Jin method [16]. One can also use the results from the DSMC methods as the reference solutions according to Degond et al. [12]. Here N_s is set to be 10^4 constantly.

Fig. 2 shows the statistical errors induced by the number of particles N for the first order AP-DSMC and ExpRK in log-log scale. It can be observed that the errors measured by L_2 norm do not change with the Knudsen number ε and do decrease monotonically. The convergence rates of each of macroscopic variables approximately equal to 1/2 for both our new method and the ExpRK method. The results are consistent with those of the conventional DSMC method in [5] and [12]. For the errors induced by N , Degond et al. [12] concluded that with some moment-guided modifications, which apply higher resolution of the thermodynamical equilibrium, one can increase the convergence rates to one. But those modifications are out of consideration in this work.

4.2. Numerical Test 2: Sod's shock tube problem

Sod's problem is wildly used to test the capability of capturing unsteady profiles and resolution of shock wave and contact discontinuity. Now we conduct simulations of this problem with various Knudsen number from $\varepsilon = 10^0$ to 10^{-6} . The aim is (1) to test the numerical capabilities of the new method; (2) to compare our new method with other AP schemes. In this test, two initial data are considered to investigate the performance of AP schemes with resolved solutions and under-resolved solutions.

4.2.1. The initial data

First, the data is initialized with the Maxwellian distributions with [16, 39] (named as RUN-1)

$$\begin{cases} (\rho, u, T)_L = (1, 0, 1), & \text{if } 0 \leq x < 0.5, \\ (\rho, u, T)_R = (1/8, 0, 1/4), & \text{if } 0.5 \leq x \leq 1. \end{cases} \quad (4.4)$$

Here, DSMC, TRMC1, ExpRK, SP₃ and AP-DSMC with $\sigma_{\max} = 1.0$, 50 particles per cell, $N_s = 3 \times 10^3$, $\Delta x = 2 \times 10^{-3}$ and $\Delta t = 1.25 \times 10^{-4}$ are tested. The reference solutions are computed by the second order Filbet-Jin method [16] with $\Delta x = 10^{-3}$ and $\Delta t = 6.25 \times 10^{-5}$ for $\varepsilon = 10^{-2}$ and $\varepsilon = 10^{-4}$, and the Euler solver [28] with $\Delta t = 2.32 \times 10^{-4}$ and $\Delta x = 10^{-3}$ for $\varepsilon = 10^{-6}$. The output time is $t = 0.2$.

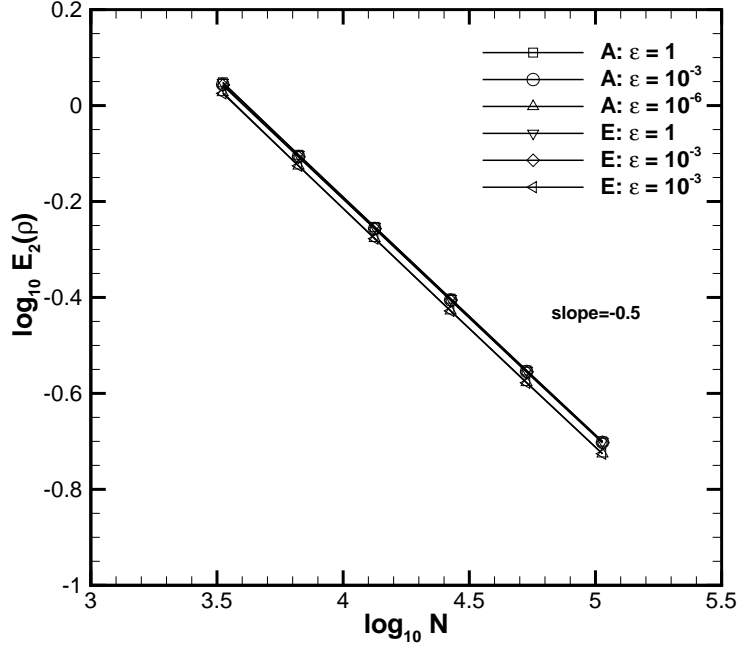


Figure 2: Statistical errors (4.3) induced by the finite number of particles with AP-DSMC (denoted as A) and ExprRK (denoted as E). Solutions at $t = 0.05$ for density. Knudsen number ε is set to 1, 10^{-3} and 10^{-6} respectively. Squares and gradients indicate errors for $\varepsilon = 1$, circles and diamonds for $\varepsilon = 10^{-3}$, deltas and left triangles for $\varepsilon = 10^{-6}$.

With another data [13] initialized with the Maxwellian distributions in the following, the performance of AP schemes with under-resolved solutions is compared. (named as RUN-2)

$$\begin{cases} (\rho, u, T)_L = (1, 0, 5), & \text{if } 0 \leq x < 0.5, \\ (\rho, u, T)_R = (1/8, 0, 4), & \text{if } 0.5 \leq x \leq 1. \end{cases} \quad (4.5)$$

Here, TRMC2, ExprRK, and AP-DSMC with $\sigma_{\max} = 1.0$, 500 particles per cell, $N_s = 10^4$, $\Delta x = 6.7 \times 10^{-3}$ and $\Delta t = 4.17 \times 10^{-4}$ are tested. The reference solutions are computed by DSMC for $\varepsilon = 10^{-3}$ and $\varepsilon = 10^{-4}$ with $\sigma_{\max} = 1.0$, 10^3 particles per cell, $N_s = 10^4$, $\Delta x = 6.7 \times 10^{-3}$ and $\Delta t = 8.33 \times 10^{-5}$. The output time is $t = 0.05$.

The Neumann boundary conditions in the x -direction are applied for both RUN-1 and RUN-2.

4.2.2. The unsteady profiles

In Fig. 3, comparisons of macroscopic quantities (such as density) by DSMC, ExprRK, AP-DSMC and reference solutions with RUN-1 are made. Results show good agreement for different flow regimes, including the near-continuum regime ($\varepsilon = 10^{-4}$). Fig. 3 indicates that all the methods tested here can capture the positions and profiles of the expansion wave, contact discontinuity and shock wave in all the flow regimes, including near continuum regime. Other methods show the same results which are not plotted here for clarity. Note that even with the mesh size and time step larger than ε when $\varepsilon \rightarrow 0$, ExprRK, SP₃, AP-DSMC and TRMC1 have the asymptotic-preserving properties. On the other hand, for this run, no obvious differences between AP-DSMC and ExprRK or TRMC1 in accuracy are observed in all regimes. Therefore, next we will focus on the comparison in computational efficiency.

4.2.3. The computational efficiency test for RUN-1

Furthermore, the efficiency of these methods is studied. Fig. 4 shows the comparisons of the computational CPU time of DSMC, ExprRK, TRMC1, SP₃ and AP-DSMC. ε varies from 10^0 to 10^{-6} .

When $\varepsilon \sim O(1)$, there is almost no difference between DSMC and other methods (only AP-DSMC and ExprRK are plotted in this regime). However, the computational cost of DSMC starts to soar after ε decreases to 10^{-4} and becomes

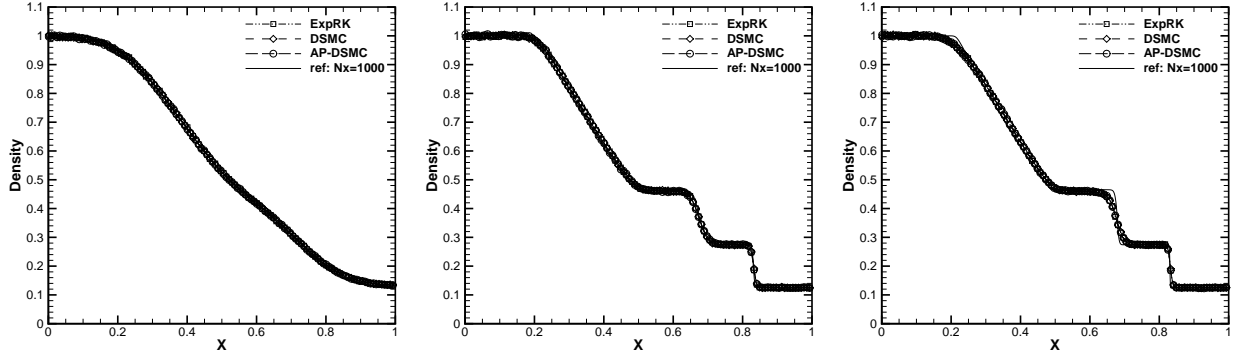


Figure 3: The comparison of density at $t = 0.2$ and $\varepsilon = 10^{-2}$ (left), $\varepsilon = 10^{-4}$ (middle) and $\varepsilon = 10^{-6}$ (right) for the Sod's problem with RUN-1. Solid lines indicate the reference solutions by the second order Filbet-Jin method [16] for $\varepsilon = 10^{-2}$ and $\varepsilon = 10^{-4}$, while the reference solutions are computed by the Euler solver [28] for $\varepsilon = 10^{-6}$. The squares are given by the ExprRK method, the diamonds are given by the DSMC method, and the circles by the first order AP-DSMC method. For simplicity, only 1 of every 5 mesh points is plotted for these three methods.

unacceptably expensive when $\varepsilon \rightarrow 0$. Since ExprRK, TRMC1, SP₃ and AP-DSMC are asymptotic preserving, they perform much better than DSMC near the continuum flow regimes. On the other hand, there are notable differences in efficiency between AP-DSMC and exponential schemes (ExprRK and TRMC1) when $\varepsilon \ll 1$, even though they share the same performance when $\varepsilon \ll 1$. It should be noticed that for $\varepsilon = 10^{-4}$ and $\varepsilon = 10^{-5}$, the value of $\bar{\mu}$ ($= \frac{1}{nt_{out} \cdot MNC} \sum_{n=1}^{nt_{out}} \sum_{i=1}^{MNC} \mu_i^n$), where nt_{out} is the number of time steps, is in the range of [1, 10] where the value of $\Theta(\bar{\mu})$ defined in (3.25) is larger than 0. Note that μ_i^n is the value of μ defined in (2.10) at the n -th time step and the i -th cell.

Table 4.1 gives the specific cost of the colliding part T_{coll} (see Eqn. (3.11), *colliding* part), the relaxation part T_M and the total running time T_{tot} for different methods for $\varepsilon = 10^{-5}$. ξ_0 in Table 4.1 is positive and negligible. As mentioned in section 3, the computational cost of DSMC and AP-DSMC depends on $\bar{\mu}$, and when $\bar{\mu} \gg 1$, the cost taken by DSMC becomes unacceptable, which complies with the discussion in section 3.3. In this case, $\bar{\mu} \approx 7$, so the cost of DSMC is not extremely expensive. However, from Fig. 4, when ε decreases further, $\bar{\mu}$ increases, which causes the computational cost of DSMC arise dramatically.

Table 4.1: Comparisons of computational CPU time (in hrs) taken by different methods for $\varepsilon = 10^{-5}$ with RUN-1

| Name | T_{coll} | T_M | T_{tot} |
|-----------------|------------|-------|-----------|
| DSMC | 11.16 | – | 11.52 |
| ExprRK | 0.05 | 4.67 | 5.40 |
| TRMC1 | ξ_0 | 4.68 | 5.33 |
| SP ₃ | 0.32 | 4.06 | 5.15 |
| AP-DSMC | 0.45 | 3.35 | 4.55 |

It can be seen in Table 4.1 and Fig. 4 that

1. The computational costs taken by DSMC is about twice as much as that of all other methods, and the relaxation part costs much more computational time than the collision part for all AP schemes;
2. ExprRK and TRMC1 share a similar efficiency in all the flow regimes; (hence TRMC1 will not be considered in the following.)
3. AP-DSMC is more efficient than other methods in the near continuum regime, i.e. time used by AP-DSMC is around 15% less than that by ExprRK.

4.2.4. The computational efficiency test for RUN-2

The aim of this part is to compare AP-DSMC with the second order time accurate time relaxed method (TRMC2) in computational efficiency with similar results or numerical errors. Fig. 5 shows the density and heat flux (1.11)

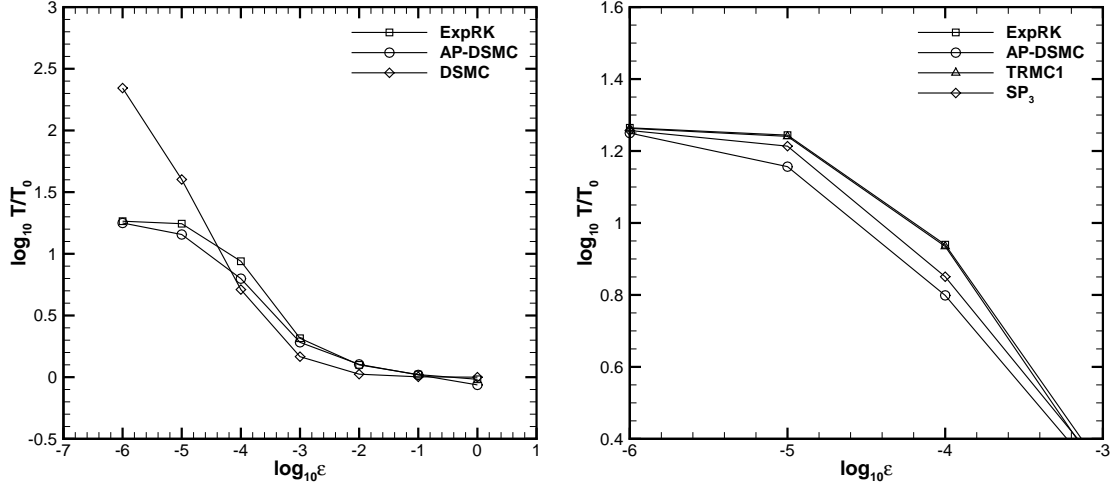


Figure 4: Comparisons of the computational efficiency of DSMC, ExprRK, TRMC1, SP₃ and AP-DSMC when the Knudsen number varies from $\varepsilon = 10^0$ to $\varepsilon = 10^{-6}$ with RUN-1. Diamonds indicate DSMC, squares for ExprRK, deltas for TRMC1, diamonds for SP₃ and circles for AP-DSMC. T_0 is the time taken by DSMC at $\varepsilon = 10^0$.

by AP-DSMC, ExprRK, TRMC2 and DSMC, when $\varepsilon = 10^{-3}$ and $\varepsilon = 10^{-4}$ with RUN-2. In this run, under-resolved solutions are given, and it can be observed from Fig. 5 that density profiles agree with each other well for both ε while the heat flux profiles reveal the differences in accuracy for $\varepsilon = 10^{-4}$. Specifically, AP-DSMC captures better heat flux profiles than ExprRK, which can be attributed to the different weights. On the other hand, although possessing the exponential structures of the weights, the second order time discretization method, TRMC2, can obtain a similar result as AP-DSMC. However, simulations by AP-DSMC need 2.62 hrs while TRMC2 requires 3.44 hrs. Note that, higher order time discretization methods of ExprRK or TRMC can improve the numerical results, as concluded in [13, 29], despite of taking more computational cost. In the following, TRMC2 or higher order time relaxed schemes will be out of consideration since the issue of high order time discretizations is beyond the scope of this paper.

4.3. Numerical Test 3: Mixing regime problem

This case is from Filbet and Jin [16], where the Boltzmann equation with the Knudsen number ε depending on the space variable in a wide range of mixing scales is considered.

4.3.1. The initial data

Here, the initial data is defined by (4.1), and ε is set to increase smoothly from ε_0 to $O(1)$, then jump back to ε_0 ,

$$\varepsilon(x) = \begin{cases} \varepsilon_0 + \frac{1}{2} (\tanh(16 - 20x) + \tanh(-4 + 20x)) & x \leq 0.7 \\ \varepsilon_0 & x > 0.7 \end{cases} \quad (4.6)$$

with $\varepsilon_0 = 5 \times 10^{-4}$. To avoid the influence from the boundary, we take periodic boundary condition in x .

The solutions given by our new AP-DSMC with $\sigma_{\max} = 1.0$, 50 particles per cell, $N_s = 10^4$, $\Delta x = 2 \times 10^{-3}$ and $\Delta t = 1.25 \times 10^{-4}$ is compared with the reference solutions by DSMC with $\sigma_{\max} = 1.0$, 50 particles per cell, $N_s = 10^4$, $\Delta x = 10^{-3}$ and $\Delta t = 6.25 \times 10^{-5}$. The output time is 0.25, 0.5 and 0.75.

4.3.2. The unsteady profiles

Fig. 6 shows the comparison results (density, velocity and temperature). It can be observed that our method agree with the reference method very well. This case demonstrates that AP-DSMC is capable of capturing the time dependent macroscopic quantities when ε varies in space.

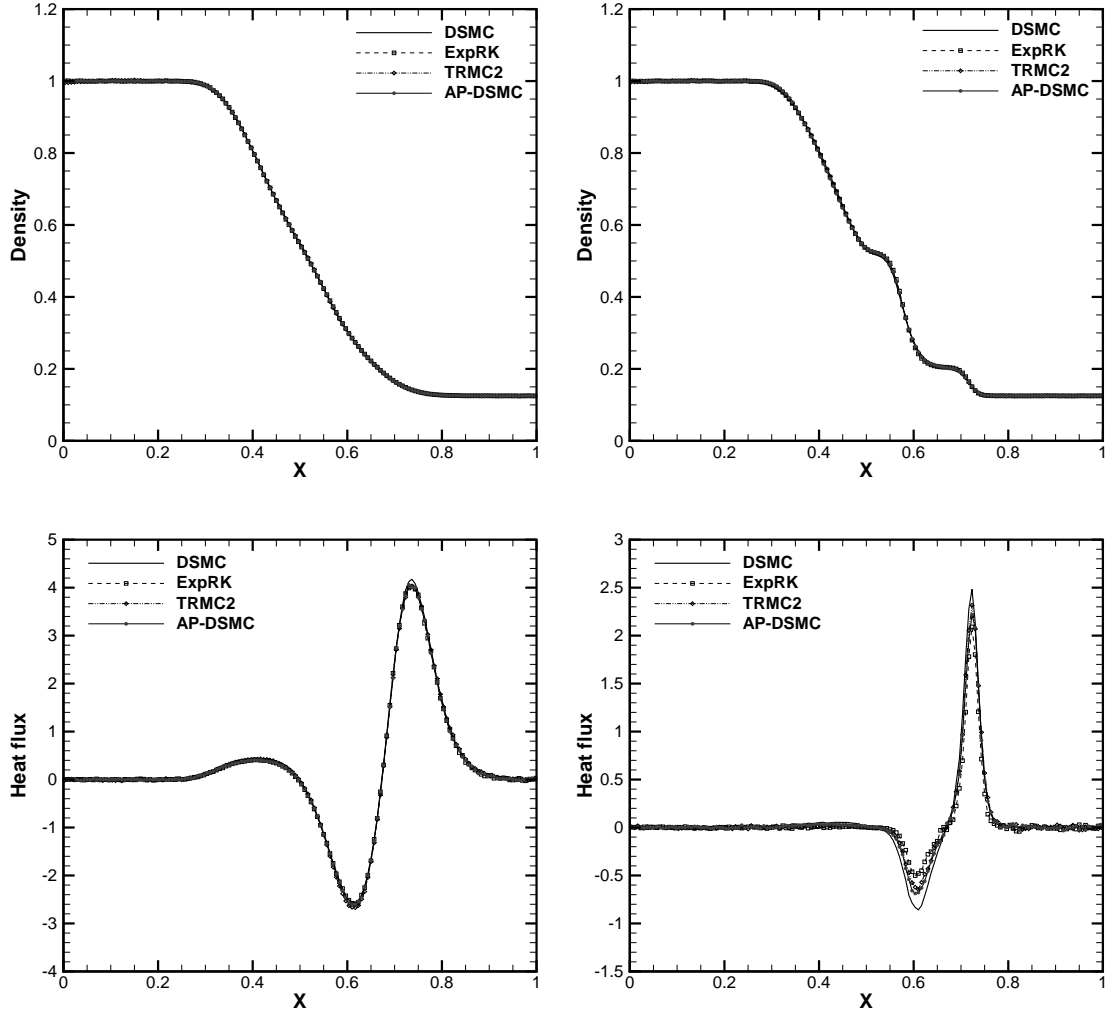


Figure 5: The comparison of density (top) and heat flux (1.11) (bottom) at $t = 0.05$ when $\varepsilon = 10^{-3}$ (left) and $\varepsilon = 10^{-4}$ (right) with RUN-2.

4.4. Numerical Test 4: The stationary shock profile problem

In this test, the stationary shock profiles of the argon gas (at $293K$) at different shock Mach numbers are simulated by our new AP-DSMC. The reference solutions are computed by *DSMCIS.FOR* [5]. The aim of this case is to investigate the ability of simulating the real gas flows by our method. The computational domain is $[-22.3, 22.3]$, 3D in velocity space is considered.

4.4.1. The initial data

The initial data in the upstream side ($x < 0$) is given by

$$\begin{cases} \rho^0(x) = 1.0, \\ u^0(x) = \begin{pmatrix} M\sqrt{\gamma T} \\ 0 \\ 0 \end{pmatrix}, \\ T^0(x) = 1.0, \end{cases} \quad (4.7)$$

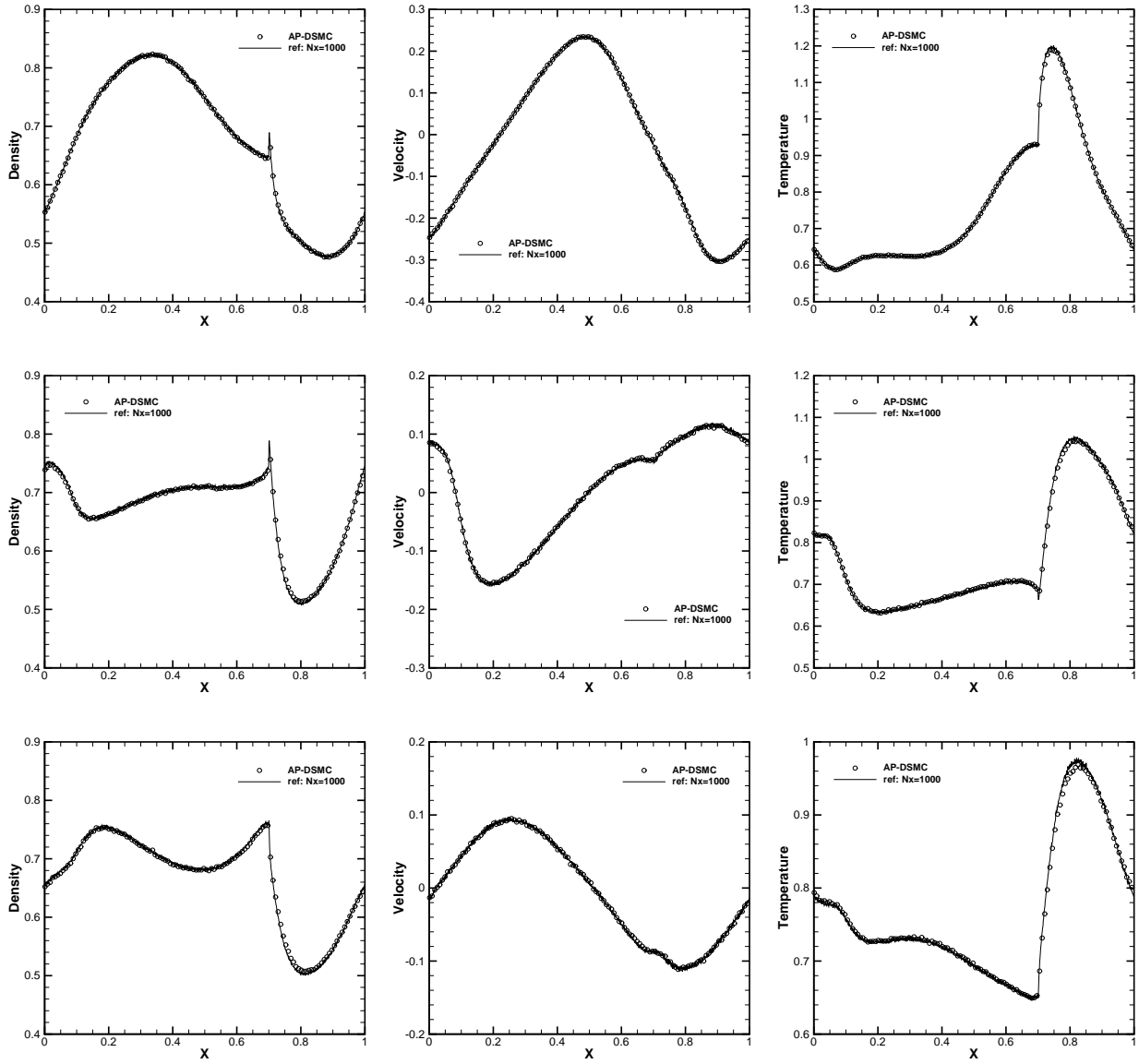


Figure 6: The comparison of density, velocity and temperature at $t = 0.25$ (top), $t = 0.5$ (middle) and $t = 0.75$ (bottom) for the mixed-regime problem. $N_x = 500$ for AP-DSMC (circles) and $N_x = 1000$ for reference solution (solid lines). For simplicity, only 1 of every 5 mesh points is plotted for all scatters.

where M is the Mach number and $\gamma = \frac{d_u+2}{d_v} = \frac{5}{3}$ is the specific ratio.

The data in the downstream side ($x > 0$) is computed by the *Rankine-Hugoniot relations* [5]. The boundary conditions of both sides are farfield conditions. The Mach number is set to be 1.4, 2.0, and 8.0 respectively. The time step is 1.344×10^{-2} and $N_x = 300$. 50 particles per cell is given in the upstream. For both DSMC and AP-DSMC, the output results are averaged by 8×10^5 samples. Here, $\varepsilon = 1.0$ and the mean free path is $\ell = 1.34 \times 10^{-2}m$. Besides, the VSS molecular model is applied and one can refer to [5] for more details.

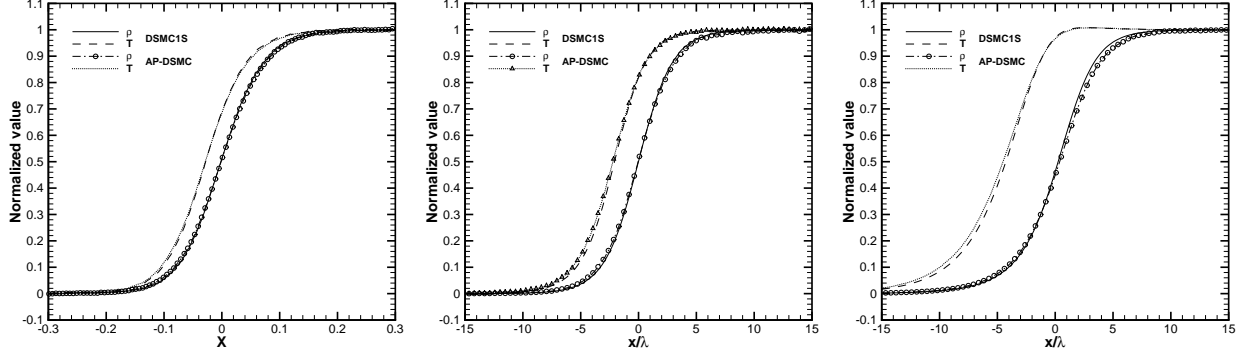


Figure 7: The stationary shock profile of argon gas at Mach number 1.4 (left), 2.0 (middle), and 8.0 (right). All the values are normalized by the initial data. The solid or dash lines are the results by the DSMC1S.FOR, while the dashdot lines with circles or dot lines with deltas indicate the computations by the AP-DSMC. For simplicity, only 1 of every 3 mesh points is plotted for these two methods.

4.4.2. The shock profiles

The results are normalized by the initial data as follows:

$$\zeta^* = \frac{\zeta - \zeta_0(x < 0)}{\zeta_0(x > 0) - \zeta_0(x < 0)}, \quad (4.8)$$

where $\zeta = (\rho, u, T)$ and $\zeta_0 = \zeta(t = 0)$.

Fig. 7 shows the stationary profile of the argon gas in $\frac{x}{\ell} \in [-15, 15]$ at Mach number 1.4, 2.0, and 8.0, which are computed by *DSMC1S.FOR* and our AP-DSMC. The results indicate very good agreement with each other.

On the other hand, one can notice that there are obvious separation of density and temperature in a shock. This is because of the finite relaxation times for momentum and energy transport [19]. From the results, it can be determined that our new method succeeds in capturing the finite relaxation times for the supersonic or hypersonic shocks.

4.4.3. The thickness of shock

To investigate the capability of the new method further, the experimental results is used as reference. Defining the reciprocal front width [14] by

$$\frac{\ell}{\delta} = \max_i \left(\frac{\rho_{i+1} - \rho_{i-1}}{2\Delta x} \right) \frac{1}{\rho_R - \rho_L}, \quad (4.9)$$

where δ is the density front width determined from the maximum of $\frac{\partial \rho}{\partial x}$.

Fig. 8 shows the comparisons between AP-DSMC with $\eta = 12$ and experimental data from [35], where η is the exponent of the intermolecular force law [4]. The solid curve in Fig. 8 from [2] is a fitting curve of their experimental results. Here $\Delta t = 4 \times 10^{-4}$, $\Delta x = 10^{-3}$, the number of particles per cell is 50, and $N_s = 2.5 \times 10^5$. In addition, the VHS model is employed. It can be observed that our results not only capture the correct tendency with increasing Mach number, but agree with the reference as well. This demonstrates the ability of the new method in simulating the realistic physical or engineering problems.

4.5. Numerical Test 5: The hypersonic flows past a cylinder problem

In this test, two-dimensional AP-DSMC schemes are investigated, and σ_{\max} is updated at each time step. The aim is to investigate the performances of AP-DSMC and ExpRK in two dimensional flows.

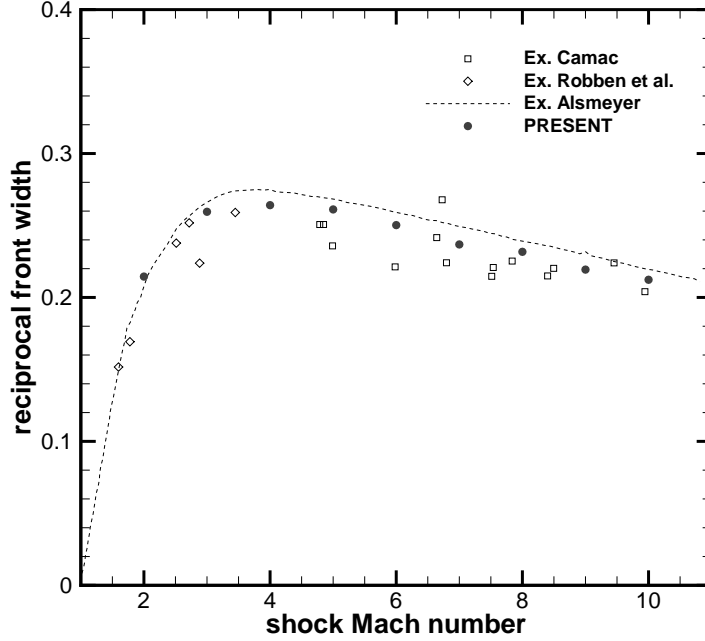


Figure 8: The reciprocal front width ℓ/δ with increasing shock Mach number M_s . All the experimental results (argon) come from [2, 35], which are compared with our new AP-DSMC method.

4.5.1. The initial data

The freestream condition is

$$\rho = 1.0, \quad T = 1.0, \quad T_{wall} = 2.0, \quad (4.10)$$

where T and T_{wall} are the freestream gas and the wall temperature, respectively. The diffusive reflection boundary condition [5, 9] is applied on the wall. The velocity can be characterized by a Mach number M :

$$u(x) = \begin{pmatrix} M \sqrt{\gamma T} \\ 0 \\ 0 \end{pmatrix}. \quad (4.11)$$

In this test, a monatomic gas is considered and $\gamma = \frac{5}{3}$. Besides, the Mach number is chosen as $M = 10$. Fig. 9 shows the geometric scale of the computational domain and the grid system used in this test. Specifically, the radius of the cylinder is $R = 0.0381m$, and the center of the cylinder (or called *forebody*, here only 1/4 cylinder is considered) is located at the origin. A spline connecting two control points $A(-1.75R, 0)$ and $B(0, 3.5R)$ is regarded as the outer farfield boundary, and the domain is closed with two additional straight lines. In this case, a structured body-fitting grid is applied, and the grid dimensions are 91×121 . The space scale of the first grid near the wall is 1.5×10^{-4} . In addition, the simulations are initialized with at least 40 particles per cell and averaged by 1×10^4 samples. The time step is 1.81×10^{-5} . As a reference solution, DSMC is computed with $\Delta t = 3.62 \times 10^{-6}$, at least 40 particles per cell and averaged by 2.5×10^4 samples.

4.5.2. Flowfields and wall information

Fig. 10 shows the contour of macroscopic quantities for AP-DSMC and Exprk when $\varepsilon = 10^{-3}$. It is observed from the contour plots that results of AP-DSMC and Exprk are almost identical, and both agree with the reference solutions very well. However, in Fig. 11, the pressure and heat transfer coefficients on the walls defined by

$$C_P = \frac{P}{\rho_0 u_0^2}, \quad C_H = \frac{\rho q_w}{\rho_0 u_0^3}$$

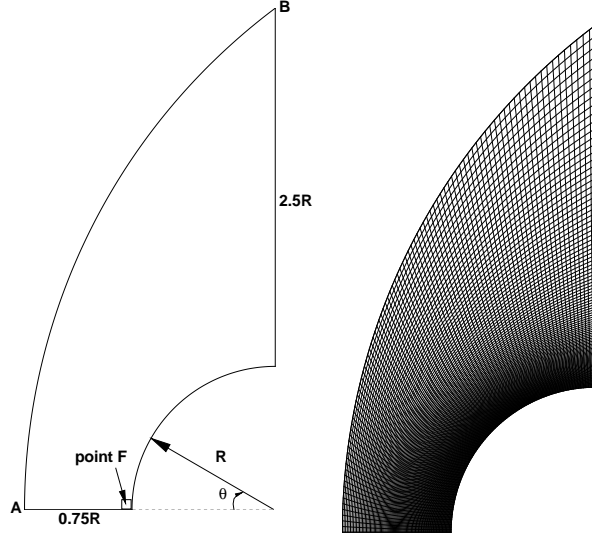


Figure 9: Schematic plot for the case (left) and the grid system (right).

are plotted for both $\varepsilon = 10^{-3}$ and ε^{-4} . Here $\theta = -\arctan\frac{y}{x}$ refers to the angle (see Fig. 9), p and ρq_w denote the pressure and heat flux on the wall, and ρ_0 and u_0 are the initial density and velocity magnitudes.

The results indicate that the pressure computed by both AP-DSMC and ExprRK are consistent with DSMC's simulations, while AP-DSMC performs better in computing the peak heat transfer when $\varepsilon = 10^{-3}$ in this test. From the plot (see Fig. 11) of the distribution function at point F in Fig. 9, AP-DSMC reproduces a more agreeable distribution function than ExprRK, and noticeable difference between AP-DSMC and the reference method can be narrowed by using a smaller time step and grid step to resolve the solutions.

On the other hand, it can be noticed that the peak heat flux value (at $\theta = 0$) of ExprRK for $\varepsilon = 10^{-3}$ complies with that for $\varepsilon = 10^{-4}$. It could be explained by the reason that ExprRK is more likely to reproduce a solution in the Euler limit rather than the Navier-Stokes limit when $\varepsilon \ll 1$, therefore it fails to compute any heat flux, which in a Maxwellian is always zero. The heat flux is due to a small deviation from a Maxwellian, that is hard to capture with all schemes based on projection onto a Maxwellian.

Therefore, this test demonstrates that in the near-continuum regime, AP-DSMC performs better than ExprRK does, especially when computing heat flux, in two-dimensional hypersonic flows simulations, and our new method is very promising in engineering applications.

4.6. Numerical Test 6: The shock-wedge problem

In this test, two-dimensional unsteady AP-DSMC schemes are investigated, and σ_{\max} is updated at each time step.

4.6.1. The initial data

Fig. 12 shows the numerical setup of this test. Here, the wedge is at 25 degree and the initial shock position is at $x = 0.18$. The computational domain is uniformly divided into 100×60 cells and the structured body-fitting grid is applied. At least 20 particles per cell are placed initially and 10^3 samples are averaged. The time step is 6.25×10^{-4} . The left boundary is inlet (or farfield) boundary condition while the other three are specular reflection boundary conditions.

Initially, the computational domain is divided into two: (1) phase I (ρ_1, u_1, p_1); and (2) phase II (ρ_2, u_2, p_2). Phase I is the stationary domain (ρ_1, u_1, p_1) = (1, 0, 1) while phase II is the post-shock domain. Here, the shock Mach number is $Ma_s = 3.0$, then $\rho_2/\rho_1 = 3.0$ and

$$\frac{p_2}{p_1} = 1 + \frac{2\gamma}{\gamma + 1} (Ma_s^2 - 1) = 11.0,$$

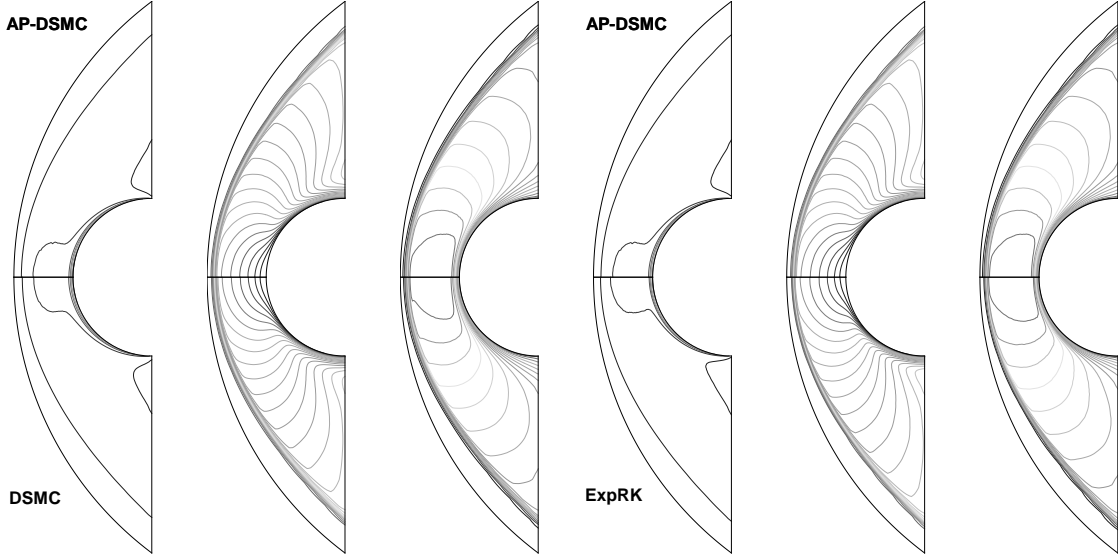


Figure 10: The contour of macroscopic quantities (density (left), velocity (middle) and temperature (right)) for each comparison, $\varepsilon = 10^{-3}$.

for $\gamma = \frac{5}{3}$. u_2 can be calculated by the following equation:

$$u_2 = \frac{a_1}{\gamma} \left(\frac{p_2}{p_1} - 1 \right) \sqrt{\frac{\frac{2\gamma}{\gamma+1}}{\frac{p_2}{p_1} + \frac{\gamma-1}{\gamma+1}}} = 2.582, \quad (4.12)$$

where $a_1 = \sqrt{\gamma \frac{p_1}{\rho_1}}$ is the speed of sound in phase I. One can refer to [8] for more details.

4.6.2. Unsteady flowfields

Fig. 13 and Fig. 14 show the contour of density at $\varepsilon = 10^{-2}$ and $\varepsilon = 10^{-4}$, respectively. The output time is $t = 0.05$, $t = 0.1$ and $t = 0.15$. Both AP-DSMC and ExpRK are tested here. From the contour, both methods capture the moving shock wave and the reflected waves. To be more specific, the profiles of density of the near wall grids are plotted in Fig. 15. It is shown that for both $\varepsilon = 10^{-2}$ and $\varepsilon = 10^{-4}$, the results of two methods are almost the same in accuracy.

4.6.3. Efficiency in two-dimensional cases

Furthermore, the computational efficiency of both methods are compared here. Table 4.2 gives the CPU time taken at $\varepsilon = 10^{-2}$, 10^{-3} , 10^{-4} . It is clear that when ε diminishing, the deviations in time between ExpRK and AP-DSMC are narrowed. For the case of $\varepsilon = 10^{-2}$, AP-DSMC only took 74% time of ExpRK. Hence, this case confirm that the computational efficiency of AP-DSMC can be over 20% more than ExpRK when the macroscopic quantities agree with each other.

Table 4.2: Comparisons of computational CPU time (in hrs) taken by different methods

| Name | $\varepsilon = 10^{-2}$ | $\varepsilon = 10^{-3}$ | $\varepsilon = 10^{-4}$ |
|---------|-------------------------|-------------------------|-------------------------|
| ExpRK | 20.02 | 24.43 | 24.30 |
| AP-DSMC | 14.83 | 22.46 | 24.58 |

5. Conclusions

In this paper we have introduced a new asymptotic preserving Monte Carlo method for the Boltzmann equation based on the successive BGK penalty methods introduced in [39]. This scheme allows time step and particle numbers independent of the Knudsen number, thus is much more efficient than the classical DSMC methods in the fluid dynamical regimes. It is also slightly more efficient than other AP-DSMC methods based on exponential Runge-Kutta methods since it puts less weight on the sampling of the local Maxwellian. In addition, with under-resolved solutions, AP-DSMC performs better than ExpRK at a moderately small ε , especially for heat flux computations, while higher order time discretization methods can improve the results, as concluded in [13, 29]. We also extended it to 2D in space, and compared with the open source code *DSMCIS.FOR* by G.A. Bird, which demonstrates its ability of solving problems involving the real gas properties, which is of importance in hypersonic flows. Various numerical examples show that the method can capture the dynamics of the Boltzmann equation in all range of Knudsen numbers.

In the future, we will work on improving the numerical accuracy of our method with low-deviation techniques and applying the method in more complicated engineering problems.

6. Acknowledgment

The first author would like to thank Dr. Qin Li for some helpful discussion on exponential Runge-Kutta methods, and Dr. Bokai Yan for providing the code of spectral method for the collision term. We also thank the referees for their constructive comments which allow us to improve the quality of the paper.

References

- [1] F.J. Alexander, A.L. Garcia, B.J. Alder, Cell size dependence of transport coefficients in stochastic particle algorithms, *Physics of Fluids* 10 (1998) 1540–1542.
- [2] H. Alsmeyer, Density profiles in argon and nitrogen shock waves measured by the absorption of an electron beam, *Journal of Fluid Mechanics* 74 (1976) 497–513.
- [3] H. Babovsky, On a simulation scheme for the Boltzmann equation, *Mathematical Methods in the Applied Sciences* 8 (1986) 223–233.
- [4] G.A. Bird, Aspects of the structure of strong shock waves, *Physics of Fluids* 13 (1970) 1172–1177.
- [5] G.A. Bird, *Molecular gas dynamics and the direct simulation monte carlo of gas flows*, Clarendon Press, 1994.
- [6] I.D. Boyd, J.P.W. Stark, A comparison of the implementation and performance of the Nanbu and Bird direct simulation Monte Carlo methods, *Physics of Fluids* 30 (1987) 3661–3668.
- [7] J.M. Burt, I.D. Boyd, A low diffusion particle method for simulating compressible inviscid flows, *Journal of Computational Physics* 227 (2008) 4653–4670.
- [8] H.M. Cave, J.S.W. K.-C. Tseng, M.C. Jermy, J.C. Huang, S.P. Krumdieck, Implementation of unsteady sampling procedures for the parallel direct simulation Monte Carlo method, *Journal of Computational Physics* 227 (2008) 6249–6271.
- [9] C. Cercignani, *The Boltzmann equation and its applications*, Springer-Verlag, 1988.
- [10] S. Chapman, T.G. Cowling, *The mathematical theory of non-uniform gases*, Cambridge University Press, 1991.
- [11] G. Chen, I.D. Boyd, Statistical error analysis for the Direct Simulation Monte Carlo Technique, *Journal of Computational Physics* 126 (1996) 434–448.
- [12] P. Degond, G. Dimarco, L. Pareschi, The moment guided Monte Carlo method, *International Journal for Numerical Methods in Fluids* 67 (2011) 189–213.
- [13] G. DiMarco, L. Pareschi, Exponential Runge-Kutta methods for stiff kinetic equations, *SIAM Journal on Numerical Analysis* 49 (2011) 2057–2077.
- [14] T.G. Elizarova, I.A. Shirokov, Simulating Argon, Helium, and Nitrogen shock waves, *Computational Mathematics and Modeling* 16 (2005) 336–348.
- [15] F. Filbet, J. Hu, S. Jin, A numerical scheme for the quantum Boltzmann equation with stiff collision terms, *ESAIM Math. Model. Numer. Anal.* 46 (2012) 443–463.
- [16] F. Filbet, S. Jin, A class of asymptotic-preserving schemes for kinetic equations and related problems with stiff sources, *Journal of Computational Physics* 229 (2010) 7625–7648.
- [17] E. Gabetta, L. Pareschi, G. Toscani, Relaxation schemes for nonlinear kinetic equations, *SIAM Journal on Numerical Analysis* 34 (1997) 2168–2194.
- [18] A. Garcia, W. Wagner, Time step truncation error in direct simulation Monte Carlo, *Physics of Fluids* 12 (2000) 2621–2633.
- [19] C.J. Greenshields, J.M. Reese, The structure of shock waves as a test of Brenner’s modifications to the Navier-Stokes equations, *Journal of Fluid Mechanics* 580 (2007) 407–429.
- [20] N.G. Hadjiconstantinou, Analysis of discretization in the direct simulation Monte Carlo, *Physics of Fluids* 12 (2000) 2634–2638.
- [21] N.G. Hadjiconstantinou, A.L. Garcia, M.Z. Bazant, G. He, Statistical error in particle simulations of hydrodynamic phenomena, *Journal of Computational Physics* 187 (2003) 274–297.

- [22] M. Ivanov, G. Markelov, S. Gimelshein, Statistical simulation of reactive rarefied flows - Numerical approach and applications, 7th AIAA/ASME Joint Thermophysics and Heat Transfer Conference AIAA Paper 1998-2669 (1998).
- [23] S. Jin, Efficient asymptotic-preserving (AP) schemes for some multiscale kinetic equations, *SIAM Journal on Scientific Computing* 21 (1999) 441–454.
- [24] S. Jin, Asymptotic preserving (AP) schemes for multiscale kinetic and hyperbolic equations: a review, Lecture Notes for Summer School on "Methods and Models of Kinetic Theory" (M&MKT), Porto Ercole (Grosseto, Italy), *Rivista di Matematica della Università di Parma* 3 (2012) 177–216.
- [25] S. Jin, B. Yan, A class of asymptotic-preserving schemes for the Fokker-Planck-Landau equation, *Journal of Computational Physics* 230 (2011) 6420–6437.
- [26] K.C. Kannenberg, I.D. Boyd, Strategies for Efficient Particle Resolution in the Direct Simulation Monte Carlo Method, *Journal of Computational Physics* 157 (2000) 727–745.
- [27] G. LeBeau, A parallel implementation of the direct simulation monte carlo method, *Computer Methods in Applied Mechanics and Engineering* 174 (1999) 319–337.
- [28] R.J. LeVeque, *Numerical Methods for Conservation Laws*, Lectures in Mathematics, ETH-Zurich, Birkhauser-Verlag, Basel, 1990.
- [29] Q. Li, L. Pareschi, Exponential Runge-Kutta schemes for inhomogeneous Boltzmann equations with high order of accuracy, *Journal of Computational Physics* 259 (2014) 402–420.
- [30] M.N. Macrossan, The Equilibrium Flux Method for the calculation of flows with non-equilibrium chemical reactions, *Journal of Computational Physics* 80 (1989) 204–231.
- [31] L. Pareschi, R.E. Caflisch, An Implicit Monte Carlo Method for Rarefied Gas Dynamics, *Journal of Computational Physics* 154 (1999) 90–116.
- [32] L. Pareschi, G. Russo, Time Relaxed Monte Carlo Methods for the Boltzmann Equation, *SIAM Journal on Scientific Computing* 23 (2001) 1253–1273.
- [33] L. Pareschi, S. Trazzi, Numerical solution of the Boltzmann equation by time relaxed Monte Carlo (TRMC) methods, *International Journal for Numerical Methods in Fluids* 48 (2005) 947–983.
- [34] D.I. Pullin, Direct simulation methods for compressible inviscid ideal-gas flow, *Journal of Computational Physics* 34 (1980) 231–244.
- [35] B. Schmidt, Electron beam density measurements in shock waves in argon, *Journal of Fluid Mechanics* 39 (1969) 361–373.
- [36] C. Villani, H-Theorem and beyond: Boltzmann's entropy in today's mathematics, H-Theorem and beyond: Boltzmann's entropy in today's mathematics, European Mathematical Society, 2007, pp. 129–144.
- [37] E. Wild, On Boltzmann's equation in the kinetic theory of gases, *Mathematical Proceedings of the Cambridge Philosophical Society* 47 (1950) 602–609.
- [38] R.G. Wilmoth, R.A. Mitcheltree, J.N. Moss, Zonally Decoupled Direct Simulation Monte Carlo Solutions of Hypersonic Blunt-Body Wake Flows, *Journal of Spacecraft and Rockets* 31 (1994) 971–979.
- [39] B. Yan, S. Jin, A successive penalty-based asymptotic-preserving scheme for kinetic equations, *SIAM Journal on Scientific Computing* 35 (2012) 150–172.

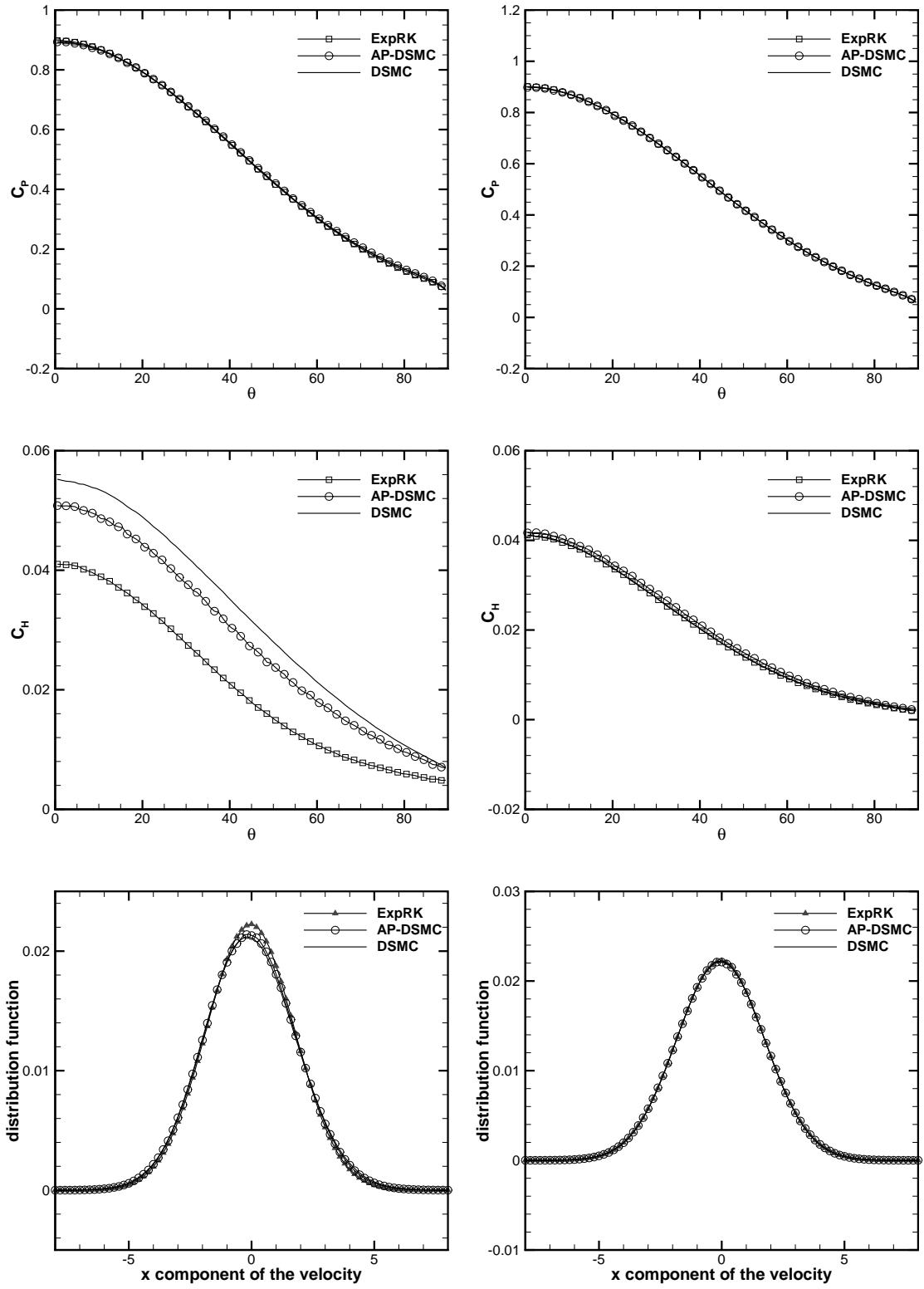


Figure 11: The wall information of AP-DSMC (circles) and ExpRK (deltas) simulations at $\varepsilon = 10^{-3}$ (left) and $\varepsilon = 10^{-4}$ (right). The reference solutions (black solid lines) are computed by DSMC. The bottom plots are the distribution function at the point F. For simplicity, only 1 of every 2 mesh points is plotted for all scatters.

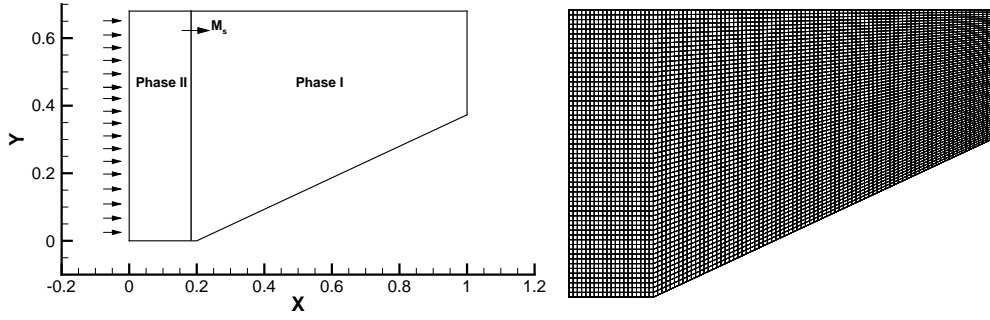


Figure 12: Setup of the shock-wedge problem (left) and the grid system (right).

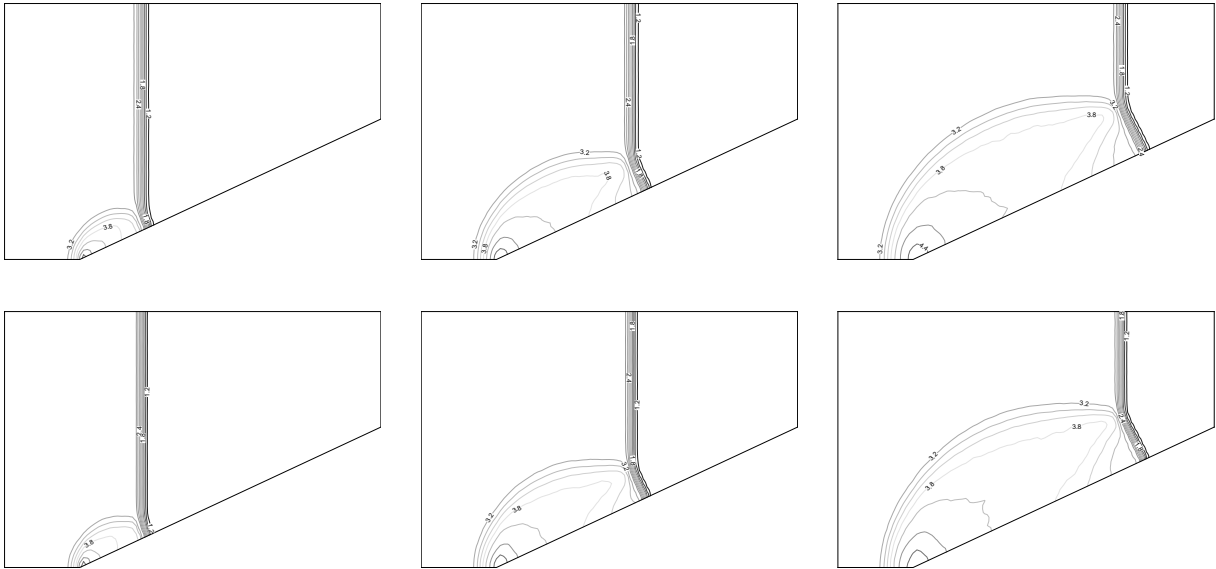


Figure 13: The contour of density ($t = 0.05$ (left), $t = 0.1$ (middle) and $t = 0.15$ (right)) at $\varepsilon = 10^{-2}$. Top: AP-DSMC and bottom: ExpRK.

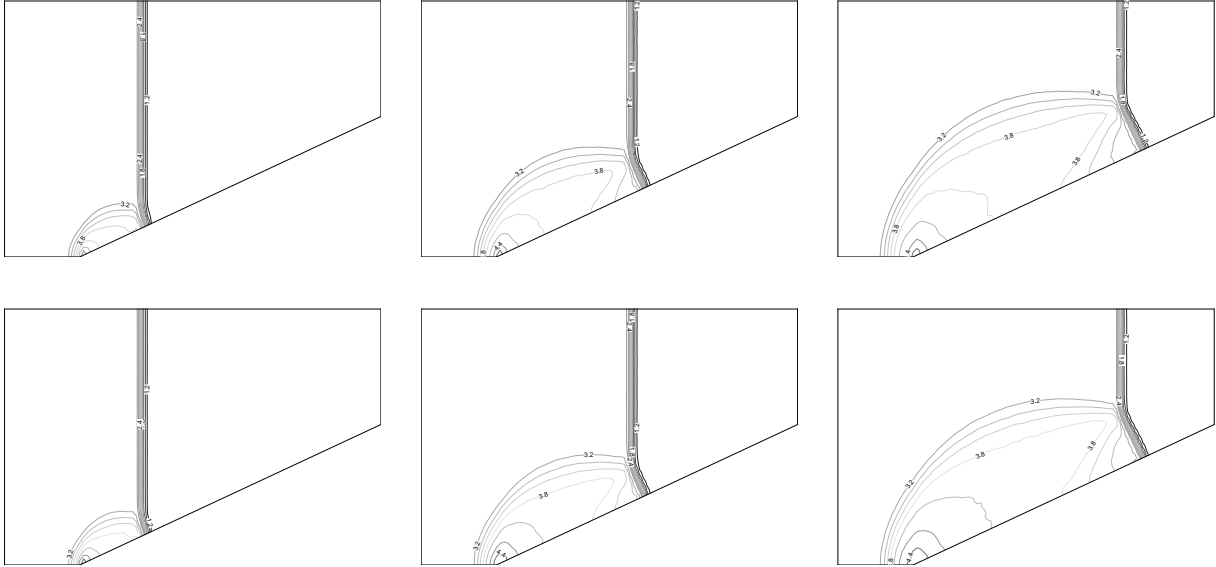


Figure 14: The contour of density ($t = 0.05$ (left), $t = 0.1$ (middle) and $t = 0.15$ (right)) at $\varepsilon = 10^{-4}$. Top: AP-DSMC and bottom: ExpRK.

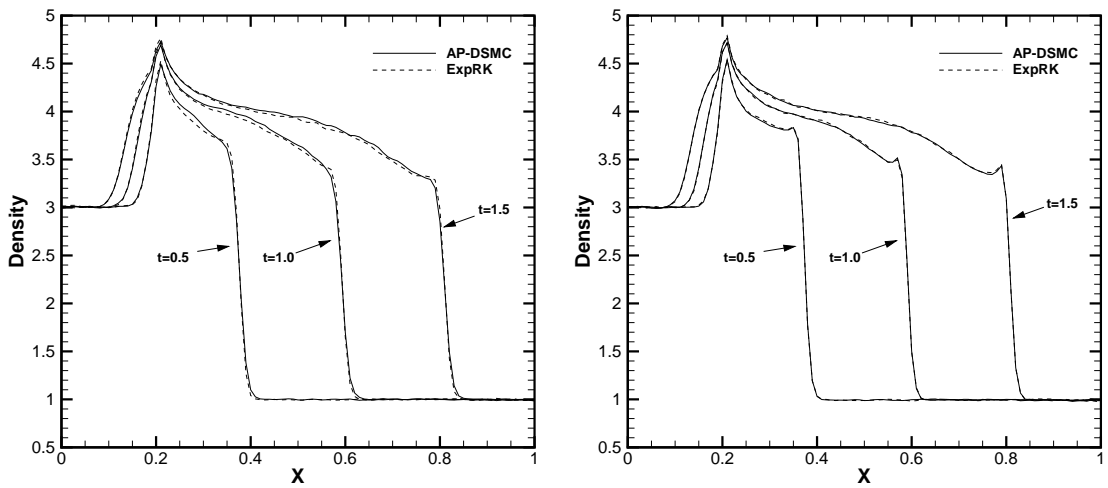


Figure 15: The profile of density along the near wall grids at $\varepsilon = 10^{-2}$ (left) and $\varepsilon = 10^{-4}$ (right).